



THE HONG KONG
POLYTECHNIC UNIVERSITY

香港理工大學

Pao Yue-kong Library

包玉剛圖書館

Copyright Undertaking

This thesis is protected by copyright, with all rights reserved.

By reading and using the thesis, the reader understands and agrees to the following terms:

1. The reader will abide by the rules and legal ordinances governing copyright regarding the use of the thesis.
2. The reader will use the thesis for the purpose of research or private study only and not for distribution or further reproduction or any other purpose.
3. The reader agrees to indemnify and hold the University harmless from and against any loss, damage, cost, liability or expenses arising from copyright infringement or unauthorized usage.

IMPORTANT

If you have reasons to believe that any materials in this thesis are deemed not suitable to be distributed in this form, or a copyright owner having difficulty with the material being included in our database, please contact lbsys@polyu.edu.hk providing details. The Library will look into your claim and consider taking remedial action upon receipt of the written requests.

**A DYNAMIC-PHYSICAL MODEL FOR LIGHTNING
RETURN STROKE CURRENT AND LIGHT
SIMULATIONS AND ITS COMPARISON WITH
OBSERVATIONS**

**CAI SHUYAO
Ph.D**

The Hong Kong Polytechnic University

2018

**The Hong Kong Polytechnic University
The Department of Building Services Engineering**

**A Dynamic-Physical Model for lightning Return
Stroke Current and Light Simulations and Its
Comparison with Observations**

CAI Shuyao

**A thesis submitted in partial fulfilment of the
requirements for the degree of Doctor of
Philosophy**

September 2017

Certificate of Originality

I hereby declare that this thesis is my own work and that, to the best of my knowledge and belief, it reproduces no material previously published or written, nor material that has been accepted for the award of any other degree or diploma, except where due acknowledgement has been made in the text.

_____ (Signed)

CAI Shuyao _____ (Name of student)

Abstract

A Lightning flash during a thunderstorm may occur either within the cloud (CC) or between the cloud and ground (CG). A CG usually starts with a leader process followed by a return stroke process. It is this return stroke that produces strong electric current pulses, which may cause damages to various systems on earth.

Observation is the most direct and accurate way to understand the property of a lightning return stroke but with limitations and various difficulties in practice. For this sake, various physical and engineering models have been proposed since 1970s to predict the properties of the return stroke parameters with various conditions. A downward lightning flash usually starts with a downward leader and an upward connecting leader followed by an upward return stroke. It is the preceding leader that governs the following return stroke property. Besides, the return stroke property evolves with height and time. These two aspects, however, are not well-addressed in most existing return stroke models.

In this study, we present a leader-return stroke consistent model based the time domain electric field integral equation (TD-EFIE), which is a growth and modification of Kumar's macroscopic model. It is a dynamic physical model that could describe the spatial and temporal evolutions of the most important parameters of a lightning return stroke, such as the lightning channel radius and conductance, the lightning current and its propagation in the channel. The model is further extended to simulate the optical and electromagnetic emissions of a return stroke by introducing a set of equations relating the return stroke current and conductance to the optical and electromagnetic emissions. With a presumed leader

initiation potential, the model can then simulate the temporal and spatial evolution of the current, charge transfer, channel size and conductance of the return stroke, furthermore the optical and electromagnetic emissions. The model is tested with different leader initiation potentials ranging from -10 to -140 MV, resulting in different return stroke current peaks ranging from 2.6 to 209 kA with different return stroke speed peaks ranging from 0.2 to 0.8 speed of light and different optical power peaks ranging from 4.76 to 248 MW/m. The larger of the leader initiation potential, the larger of the return stroke current and speed. Both the return stroke current and speed attenuate exponentially as it propagates upward. All these results are qualitatively consistent with those reported in the literature.

Publications Arising from the Thesis

Journal Paper

Shuyao CAI, Mingli CHEN, Yaping DU and Zilong QIN (2017), A leader-return-stroke consistent macroscopic model for calculations of return stroke current and its optical and electromagnetic emissions, *J. Geophys. Res. Atmos.*, **122**.
Doi:10.1002/2017JD026490.

Conference Paper

Mingli CHEN, **Shuyao CAI** and Yaping DU, Dynamic modelling of lightning return stroke and its optical and electromagnetic radiations based on Maxwell's integral-equations, *7th Asia-Pacific Conf. on Environmental Electromagnetics (CEEM)*, Nov. 4-7, 2015, Hangzhou, China. DOI: 10.1109/CEEM.2015.7368663.

Mingli CHEN, Ming-Kit CHAN, **Shuyao CAI** and Yaping DU, Macroscopic physical models for lightning leaders and return strokes, *Int. Symposium on Topical Problems of Nonlinear Wave Physics (NWP2017)*, July 22-28, 2017, Moscow, Russia.

Acknowledgements

I would like to express my sincere appreciation to my supervisor, Dr. Mingli CHEN, for his patient guidance and valuable assistance in bring out this dissertation.

I would also like to thank Prof. Yaping DU, Dr Tao LU, Dr Yanchi SHEN, Dr Yazhong XU, Miss Xueyun DING and Dr Zilong QIN, for their constant encouragement and helpful assistance during the past 5 years.

Finally, I would like to thank my family and friends, for their support in mu PhD study.

Table of Contents

Abstract	...3
Publications arising from the thesis	...5
Acknowledgements	...6
Table of Contents	...7
Chapter 1. Introduction	...9
1.1 Overview of lightning	
1.2 Lightning return strokes	
Chapter 2. Literature Review	...15
2.1 Lightning return stroke and its effect	
2.2 Observations and experiments on lightning return stroke	
2.3 Modelling of lightning return strokes	
2.4 Research gaps and objectives of this project	
Chapter 3. Research Methodology – Development of Dynamic Physical Model for Lightning Return Stroke	...24
3.1 Return Stroke Channel Formation	
3.2 Initial Condition of Return Stroke Channel	
3.3 Modeling of Return Stroke Current	
3.4 Computing Scheme for Return Stroke Modeling	
3.4.1 Numerical solution for the current	
3.4.2 Evolution of the channel conductance	

3.5 Modeling of Light and Electromagnetic Emissions of Return Stroke

3.5.1 Electrical and Magnetic Fields from Return Stroke

3.5.2 Light Emission from Return stroke

Chapter 4. Simulation Results and Its comparisons with the observations ...40

4.1 Return Stroke Current and Conductance

4. 2 Electrical and Magnetic Fields from Return Stroke

4.3 Light Emissions from Return stroke

Chapter 5. Preliminary Study of Lightning Light Spectra for Possible Model Validation. ...54

5.1 Method for Estimation of Channel Temperature from Light Spectra

5.1.1. Line spectra of lightning

5.1.2. Temperature dependence of spectra lines

5.1.3 Temperature dependence of electrical conductivity

5.2 Light Spectrum of Lightning Return Stroke

5.2.1 Existing data from America

5.2.2 Our plans for observations of lightning light spectra

Chapter 6. Conclusions and Discussion ...61

References ...66

Chapter 1. Introduction

1.1 Overview of lighting

Lightning flash refers to extremely strong and long electrical discharges in the in the cloud or between cloud and ground in the atmosphere followed by a bright flash of light and huge thunders. It is more common in summer thunderstorm weather, and rarely occurs during snow in winter. It also exist during volcano eruption or atomic bomb explosion induced by air short-circuit.

On earth, lightning occurs approximately 45~50 times for a second, 1.4 billion for a year with duration of 30 millisecond. As a result of observation from satellites [Orville and Henderson, 1986], frequency of lighting on land is 10 times more than that on the sea, and is the smallest in September and February, and smallest in April and July. The geographical distribution of lightning is closely relative to change of seasons. For example, high incidence of lightning moves from northern hemisphere of earth to southern while season changes from summer to winter. Because that area of the northern hemisphere is much larger and that surface undulation is bigger, lightning in summer is more than that in winter.

Power of lightning is from 10^8 W~ 2×10^{10} W with the peak number 10^9 1GW. Less than 2% of lightning is stronger than 10GW. There are about 3 out of 1000 lightning flashes with power of $10^{11} \sim 10^{13}$ W called super-bolt. The light power of super-bolt is comparable to that of nuclear explosion in the atmosphere. Besides the low altitude

lightning, it also occurs from top of thunder cloud to stratosphere detected by aircrafts and satellites, such as red elves, spirit, and blue jet. Some observation equipment on spacecraft also prove that lightning exist on Venus, Jupiter and Saturn. The frequency of lightning on Venus is about 30 per square meter for a year, and on Jupiter is 40. Lightnings on Saturn is much lighter than that on earth, which may happen in its ring.

Due to its large current and high voltage, lightning may cause damages to human beings, animals and artificial equipment. Based on the point discharge effect, people or animals on the open flat are easily stroked by lightning. Therefore lightning protection has been an important project for us to research.

1.2 Lightning return strokes



Fig. 1.1 Photograph of cloud lightning discharge



Fig. 1.2 Photograph of cloud to ground lightning discharge

Lightning during a thunderstorm may occur between two charge centers with opposite electrodes of two thunder clouds called cloud-to-cloud lightning (CC) or within one thundercloud (IC), or between cloud charge center and the ground called cloud-to-ground lightning discharge (CG). Photos of cloud flash and CG are referred to **Fig. 1.1** and **Fig. 1.2**.

Over 50% of all natural lightning flashes are IC. And CC is much less than that. Though most lightning occurs in the cloud, it does not connect to the ground therefore the damage of which is much smaller than CG.

A CG can be either upward- or downward-triggered, and negatively or positively charged one [Rakov and Uman, 2007]. According to electrode and motion direction, there are 4 types of CG as seen in **Fig.1.3**, among which downward-triggered negative flash is over 90%. It is initiated by a negative leader moving towards the ground and transfer negative charge to the ground, and so on. Downward-triggered positive leader accounts for less than 10% of all CGs. The other two types are

triggered by upward moving leaders, which is very rare and often occurs on tops of mountains or high artificial buildings. With increasing of high buildings in the urban area, number of upward discharge has a tendency to slightly rise. And the artificial triggered lightning with rocket is also a kind of upward-triggered flash.

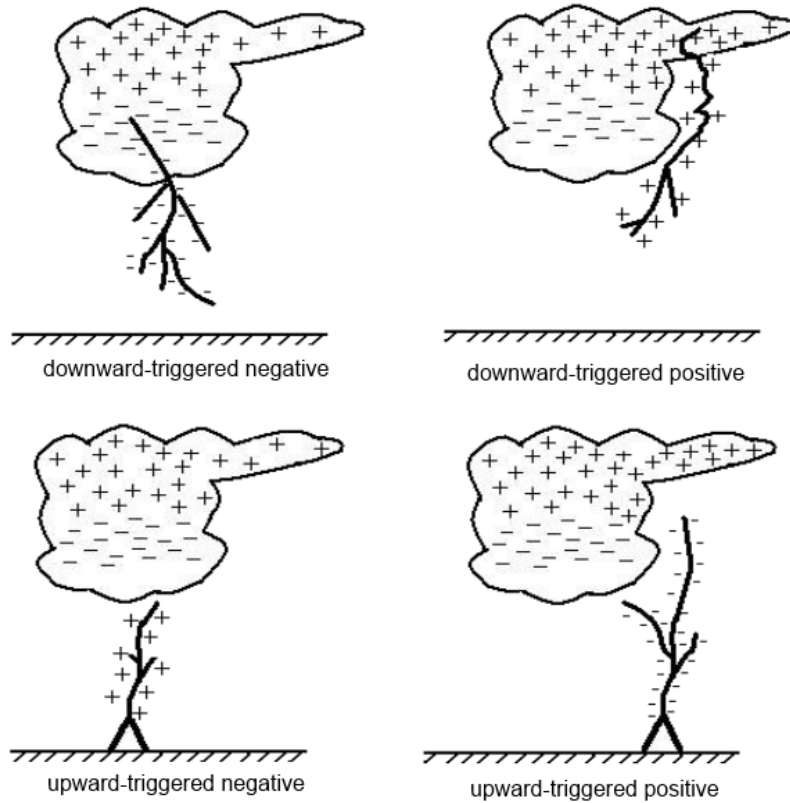


Fig. 1.3 Schematic diagram of 4 types of CG[Rakov and Uman, 2007]

A typical CG usually starts with a downward moving negatively-charged leader process, followed by an upward moving return stroke process, usually transfer tens of coulombs of negative charge to the ground. True to international tradition, a complete CG process called “a flash” or “a lightning flash”, sustains about several hundreds of milliseconds to 1 second. A flash may contains one or several high current pulse processes called “stroke”, the most strong and fast stroke is called

“return stroke”. There are tens of milliseconds of time intervals between strokes, result in twinkles appearing in our eyes.

It is this return stroke that produces very strong electric current pulse which may induce various effects on different facilities. There are about 2000 thunder storm activities every moment on the earth, result on CGs per second. Part of them strikes on all kinds of buildings artificial systems, causing harms to humans and animals. With development of human society, harms of lightning strikes become wider, extremely to microelectronic elements, increasing absolute financial loss.

In the stage of return stroke, peak current of CG may reach several tens of kilo amperes with instantaneous power higher than 10^{11} W. The energy of current pulse gives out in way of heat, mechanical energy (blast wave, sound wave, etc.), electromagnetic energy (including light energy), and so on. At that moment, the lightning channel can be heated to 30,000 centigrade by strong thermal effect of current. Only a small part is released on the ground though, strong heat and electromagnetic effect may cause large damages which make people develop protection technologies against it.

Based on statistical data of several ten years of America, lightning strike causes about 100 deaths and 500 injuries of people in the country. Researches indicate that casualties usually occur out of doors, which are regularly reduced by urbanization these years. In developed country, unprotected activities outdoors are related to sports and mining operations, while in developing countries, farming and husbandry are main areas for lightning hazards. With development of modern

industry, indirect disasters of lightning (electromagnetic damage) become especially serious. As a result, research and construction of lightning protection system is very important.

Therefore, study of the return stroke process has been a very hot topic since it has caused large damage to human life. Observation of return stroke traces back to 1774 by Franklin, including optical, acoustic and electromagnetic measurement. By analysis of these observed data, position, channel length, and some physical information of the flash can be estimated. A lot of models have been established to simulate the return stroke process based on observation results, such as physical models, electromagnetic models, engineering models and distributed-circuit models. Because of limitation of observation method and equipment, evolution of lightning return stroke such as current, conductivity, electron density, temperature, etc. is not clear to us. There is not a complete model that can describe change of all these parameters in detail.

Chapter 2. Literature review

2.1 Lightning return stroke and its effects

As has been mentioned, lightning return stroke is the most important discharge process between cloud and ground based on the fact that of all processes during a lightning flash, it is the most easily to detect for light, current, sound and electromagnetic field, and that it causes most lightning disasters to lives and facilities. In this section, the physical processes of return stroke and its effect on light, sound and electricity are to be presented.

Return stroke is the strongest discharge during the process of a CG. Take downward negative discharge for example, a typical lightning flash can be divided in the following steps, cloud charge distribution, preliminary breakdown, stepped leader, attachment process, first return stroke, K- and J- processes, dart leader, second return stroke, and so on. A lightning flash may contains several return stroke, the luminosity of a two return stroke is shown in **Fig. 2.1**.

Firstly a stepped leader starts from negative charge center in the cloud and expands downward to the ground and upward to the upper positive charge center. Before the attachment process, stepped leader generate a weak ionized channel between cloud base and ground with a constant current from several tens to hundreds

amperes. It lasts several tens of milliseconds and an upward leader may start from ground to the attachment point at the same time. The downward leader usually has many branches but only one could reach the attachment point and connect with the upward leader, initiating first return stroke process. A strong positive current pulse rises from the ground to cloud along the formed stepped leader channel with the surge of conductivity, temperature, electron density and light emitting, which is so called first return stroke of lightning. It is the huge voltage difference that causes the return stroke, which transfers a lot of positive charge to the cloud and decrease the voltage difference between cloud and ground. The duration of first return stroke is about 100 microseconds. If there is any associated in-cloud discharge activity, the flash may end. And in this case, it is called a single- stroke flash. Otherwise, dart leader and second subsequent return stroke occurs one after another. During time interval between end of the first return stroke and initiation of dart leader, K- and J- processes may occur in the cloud.

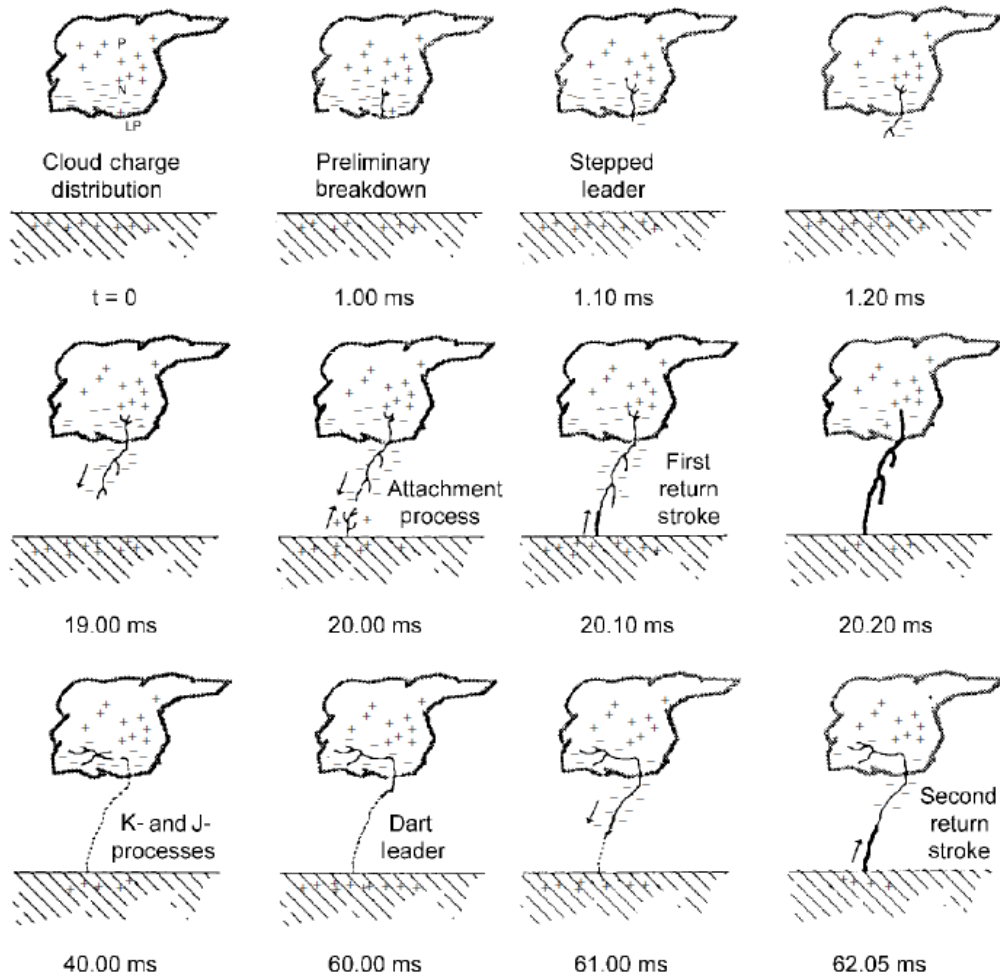


Fig. 2.1 process of a two-stroke negative CG[Uman, 2001]

The current of return stroke is related to classification of CG, stroke, geography, earth conductivity and different meteorological conditions. Karl Berger gives the most complete characterization of negative downward return strokes that strike to flat terrain and high structures shorter than 100m[K Berger, 1967]. Current wave of Berger is derived from oscillograms using resistive shunts installed on top of towers. The results presents wave shapes of average negative first and subsequent return strokes.

2.2 Observations and experiments on lightning return stroke

Lightning return strokes are defined as the acoustic and light emission associated with electric discharges between cloud and ground. There has been many experiments that measure the properties of lightning return strokes in decades.

The properties are about light, sound, and electric of return strokes. The acoustic experiments are quite few. By measuring the frequency of thunder, different types of lightning or processes can be identified. The peak of thunder power spectra of some natural CG and most cloud processes is infrasonic which is below 20Hz, while that of rocket-triggered lightning is hundreds of hertz. Acoustic recordings of thunder can also be used for the imaging of flash channels [*Rakov and Uman, 2007*].

Electric experiments about return strokes include measurements of electric field, magnetic field and current. Karl Berger and coworkers achieved current waves of triggered lightning return stroke with oscillograms using shunts installed at the top of two 70m high towers [*Karl Berger, 1975*]. Direct measurements of natural lightning return stroke currents on high towers were made by in USA [*McCann, 1944*], Germany [*Fuchs et al., 1998*], Brazil [*Pinto et al., 2005*]. The directly measured current waves aim for people's recognition of current propagation of return stroke and can be used for lightning location. Vertical and horizontal electric fields and horizontal magnetic fields produced by negative return strokes are normally necessary parameters to identify the type of a lightning process. Typical vertical electric and horizontal magnetic field waves measured from 1 km to 200 km were published [*Lin et al., 1980*], which demonstrate specified characteristics of electric and magnetic fields produced by return strokes.

Optical observations of lightning return stroke includes light intensity and spectra measurements. Propagation of light of return strokes is thought to reflect the speed and variation of current in time and space, which cannot be measured directly. Return stroke speed obtained with photographs taken by streak cameras is from $1/3 \sim 2/3$ of light speed. [Idone and Orville, 1982]. But some argues that the speed of light propagation cannot be equal to that of current propagation. According to plasma physics, luminosity of plasma gas is directly related to the temperature of it. As the energy source of heating, current must propagates faster than the temperature. D. Wang and his coworkers has provide this view by light observations [Zhou *et al.*, 2014]. Using a measuring system of with time resolution of 0.5us, Uman and Jordan [Dwyer *et al.*, 2003] found that light power of a small section of return stroke near ground channel has a fast rise to peak for about 1.5us and a slow decrease. The longest time for rise is 4us when light propagate to cloud base. Power and energy released by light of return stroke are also important parameters. The ratio of light power and electrical power is achieved by spark experiments. With the same ratio assumed, the electrical power of lightning strokes can be evaluated when the light power is measured. Guo and Krider [Guo and Krider, 1982] recorded optical signals with wavelength band of 400nm~1100nm and evaluated the peak value of light power in the distance of 5~35km.

The spectra of plasma gas indicates the temperature of it, therefore measurement of lightning spectra is an important way to study the evolution of temperature in it. Orville and Henderson used prism assembled on the camera to record the absolute spectra of lightning strokes in wavelength of 375nm~880nm [Salanave *et al.*, 1962].

By evaluating the intensity ratio between spectra lines, the temperature of lightning channel in function of time can be calculated.

2.3 Modeling of lightning return strokes

Models of lightning return stroke has been classified into 4 types[Rakov and Uman, 1998] as mentioned above. And most of models can be assigned to one or two of them.

The first class of models is physical models or gas dynamic models, which is based on three gas dynamic equations. These models study radial evolution of short segments of the lightning channel and its shock wave, showing the change of mass, momentum and energy. With input of current propagation data, the model gives out temperature, pressure and mass density versus time. Spark discharge experiment is used for establishing this type of models [Plooster, 1970; 1971; Plooster and Garvin, 1956]. Recent physical models are concerned about various type of plasma gases.

The second is electromagnetic models proposed by Landt and Moini [Moini et al., 1997; Podgorski and Landt, 1987]. Lightning channels are treated as lossy antennas in these models. Maxwell's equations are used as a numerical solution with the method of moment (MoM) [Sadiku, 2007] . With input of initial current pulse at the attachment point, these models give out complete solution of return stroke current for instance line mode current and transmission line current[Paul, 2008]. The conductivity of the channel is spatially symmetrical and temporally stable, the value

of which varies from 0.01 to 10 S/m to adjust different conditions and requirements. The complete power of

Distributed-circuit models of lightning strokes describe the lightning channels as an RLC transmission line with fixed value of resistance, inductance and capacity. The voltage and current of are calculated with telegrapher's equations. With the input current wave, propagation of return stroke current is obtained by solving the telegrapher's equations.

An engineering return stroke model is a simple equation that relate current, height and time. The equations are developed with experimental data and empirical math formulas and applied according to different engineering requirements

Kumar's model developed a macroscopic model for the first return stroke of lightning [Raysaha et al., 2011] based on electromagnetic models physical models. Physical properties such as resistivity, channel radius changes while return stroke happens. And the current propagation is evaluated by changes of electromagnetic environment. By leading the first arc equation into the model, current propagation, current, charge density, conductivity, channel radius interact with each other instead of evaluating independently. Therefore, the model is closer to the natural condition of than un-physical models with a simpler mean than gas dynamic models to get the result. The model introduced in the following chapter is based on this model and revised and improved it with observation experiment data.

2.4 Research gaps and objectives of this project

As precise physical model, gas dynamic models are too complicated to describing the temporal and spatial propagation of return stroke current, though the conductivity and radius can be estimated. The electromagnetic models are concerned about return stroke current, but the resistance of the channel is unknown and cannot describe the physical properties of the lightning channel. Similarly, distributed –circuit models and engineering models do not include any parameters of physical characteristics.

The model proposed by Kumar is includes both current characteristics. Based on electromagnetic field integration equation (EFIE), evolution of channel conductivity is added by arc regime in the model. To demonstrate change of corona sheath, charge diffusion regular is employed combined with the continuity equation. Therefore, is it a good model to describe both physical and current propagate characteristics.

However, the evolution of conductivity is unreasonable in this model. Firstly, the arcing regime referred to relatively low voltage electric discharge, as a result, the rising and falling time are worth debatable and needed to be modified. Secondly, the initial conditions such as current, conductivity and in-channel electric field are not match the measured natural conditions. And charge diffusion of corona sheath is disproportionate either.

Therefore, a new semi-physical model is proposed on the foundation of Kumar’s macroscopic model. The variation of conductivity is revised and radius of channel is

also variable to get close to the real state. Charge diffusion regular remains but the diffusion rate is adjusted according to charge density of channel core and potential difference between the inside and outside edge of the corona sheath. With the calibration of observation data, the model can be revised closer to the real condition.

Chapter 3. Research Methodology – Development of Dynamic Physical Model for Lightning Return Stroke

3.1 Return Stroke Channel Formation

As shown in **Fig.3.1**, a thundercloud usually has a typical 3 charge layer structure. A -CG usually starts with a leader process initiated at the lower part of the

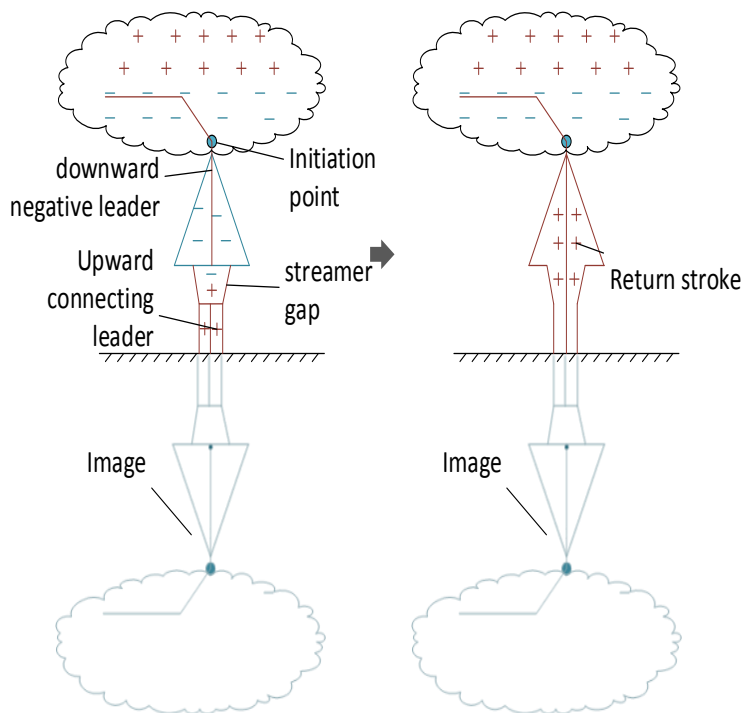


Fig. 3.1 Illustration of formation of leader-return stroke channel.

thundercloud. Subjected to the electric potential profile in and out the

thundercloud, the leader usually extends from the initiation point in both upward and downward directions. This is well-known as the bi-directional leader concept for interpretation of a variety of lightning physical process [Mazur and Ruhnke, 1998; Rioussel et al., 2007; Chen et al., 2013]. The downward part is negatively charged and propagates to ground, while the upward part is positively charged with branches stretching into the upper part of the thundercloud.

The channel of the downward leader part consists of a thin conductive core surrounded by a corona sheath. As the downward negative leader (DNL) approaches the ground, the electric field on ground increases. When the ground electric field is enhanced to the critical electrical field for positive breakdown (E_{C+}), first a positive streamer and then a positive upward connecting leader (UCL) appears there. As the UCL and DNL approach to each other. The electric field in the gap between them increases rapidly. When the electric field in the gap between the DNL and UCL reaches the critical electric field for negative breakdown (E_C), i.e. the negative streamer zone in front of the DNL touch the UCL head, a final breakdown occurs and hence a return stroke process is initiated. The return stroke usually starts with two current waves generated at the UCL and DNL connecting point, one moving upward and the other moving downward [Wang et al., 2014; Raysaha et al., 2012]. The downward wave reflects at the ground and propagates upward to catch up the previous upward wave. As the return stroke current wave propagates upward, the pre-existing leader channel is ionized further, resulting in further changes of channel radius, temperature and conductivity. The property of the return stroke basically depends on the preceding leader channel.

3.2 Initial Condition of Return Stroke Channel

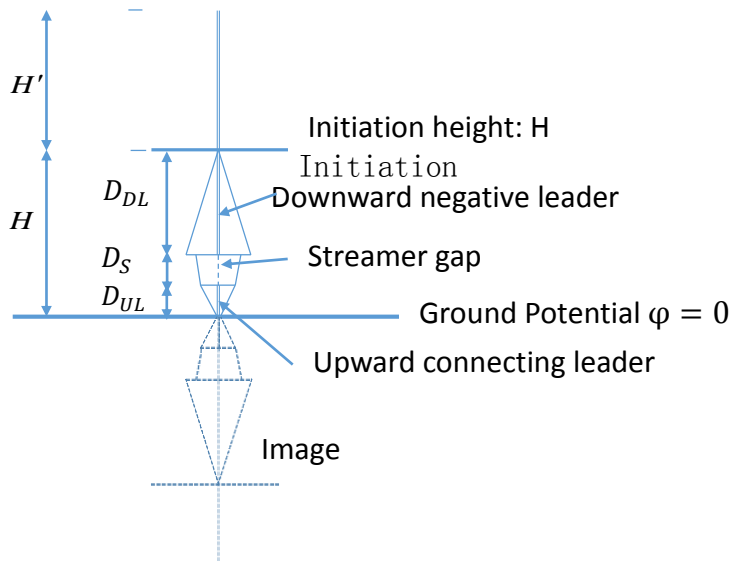


Fig. 3.2 Illustration of modeling of leader-return stroke

The condition of the preceding leader channel just before the return stroke can be taken as the initial condition of the return stroke. As shown in **Fig.3.2**, the leader channel is assumed to originate at an initiation height H with an initiation potential φ_0 and extend bi-directionally. The downward portion below the initiation height is measured H and the upward portion above the initiation height is measured H' . For the downward portion, it includes a DNL channel (D_{DL}), a UCL channel (D_{UL}) and a streamer gap (D_S). The ground is conductive and its potential is set to zero. Both the DNL and UCL channel are consisted of a thin inner core surrounded by a corona sheath. The radius of the leader core (r_0) is usually in the range of 1~5 mm and that of corona sheath may be in the range of several to tens of meters. The channel core is expected to expand after the return stroke onset and reach a few centimeters in radius [Rakov, 1998].

The late stage DNL parameters, as the initial parameters of the return stroke, are based on the leader propagation model of *Xu and Chen (2013)*. Based on that model, the leader channel line charge density $\lambda_L(z)$ (negative polarity) and corona sheath radius $r_s(z)$ in relation to the leader initiation height (H) and root potential φ_0 (negative polarity) can be simplified as:

$$\lambda_L(z) = a\lambda_0 \exp(-b \cdot z) + \lambda_0(1 - a)(1 - z/H), \quad (3.1)$$

$$r_s(z) = \lambda_L(z)/[2\pi\epsilon_0 E_C(z)], \quad (3.2)$$

$$\lambda_0 = 0.0226\varphi_0^{0.859}, \quad (3.3)$$

where, λ_0 is the leader tip charge density at its last stage just before the attachment, a a constant of about 0.6, and b a constant of about $7 \times 10^{-3} \text{ m}^{-1}$ for $H < 5000 \text{ m}$ and about $5 \times 10^{-3} \text{ m}^{-1}$ for $H \geq 5000 \text{ m}$. $E_C(z)$ is the critical electric field for negative breakdown, which is a function of the altitude above ground as $E_C = E_{CO} e^{-z/8400}$.

The length from the DNL tip to the ground when the UCL appears (D_{S+}) and the length of the streamer gap (D_s) between DNL and UCL, which is similar to the striking distance, can be estimated as:

$$D_{S+} = -\varphi_{tip}/E_{CO+}, \quad D_s = \varphi_{tip}/E_{CO}, \quad (3.4)$$

where, φ_{tip} is the DNL leader tip potential right before the return stroke, E_{CO+} (about +500 kV/m) and E_{CO} (about -750 kV/m) are the critical electrical field at ground level for positive and negative polarities, respectively. Assume that the UCL and DNL have the same speed just before the return stroke, the length of UCL can then be estimated as, $D_{UL} = (D_{S+} - D_s)/2$.

The DNL current (I_{DL}) right before the return stroke is based on the model results of *Xu and Chen (2013)* as:

$$I_{DL} = 0.1314\varphi_0^{1.502}. \quad (3.5)$$

The UCL current (I_{UL}) right before the return stroke is assumed to be a fraction of that of the DNL, say $0.3I_{DL}$. The streamer gap current (I_{ST}) right before the return stroke varies from I_{DL} when around the DNL tip down to I_{UL} when around the UCL tip.

Although the leader electric field value varies significantly over time [*Popov, 2003*], the value just before the return stroke is concerned. The longitudinal electrical field in both DNL and UCL channels just before the return stroke can be related to their leader current as:

$$E_{DL} = C_b / I_{DL}, \quad E_{UL} = C_b / I_{UL}, \quad (3.6)$$

where, C_b is a constant of about 30000 W/m based on lab experiments [*Raizer, 1991*].

The DNL tip potential is estimated as:

$$\varphi_{tip} = \varphi_0 - E_{DL}(H - D_s - D_{UL}). \quad (3.7)$$

The equivalent channel resistance per unit length of the DNL channel (Z_{DL}), the UCL channel (Z_{UL}) and the streamer gap channel (Z_{ST}), as the initial values of the return stroke channel, are estimated as:

$$Z_{DL} = E_{DL} / I_{DL}, \quad Z_{UL} = E_{UL} / I_{UL}, \quad \text{and} \quad Z_{ST} = E_{CO} / I_{ST}. \quad (3.8)$$

3.3 Modeling of Return Stroke Current

The return stroke is supposed to start when UCL and DNL accelerate within the streamer gap, producing a transient current pulse that propagates bi-directionally (downward and upward from the connection point) along the channel [Tran and Rakov, 2015]. As the downward one reaches the ground, it reflects and moves upward to catch up the previous upward one. The current propagation behavior is subjected to the total longitudinal electrical field in the channel core including the scattered field and the field due to cloud and leader charges. A time domain electric field integral equation (TD-EFIE) for solving vertical thin wire structure electromagnetic problems derived by Miller *et al.* (1973) is:

$$\hat{z} \cdot \vec{E}^A(\hat{z}, t) - \frac{\mu_0}{4\pi} \int_{C(\vec{z})} \left[\begin{array}{c} \frac{\hat{z} \cdot \hat{z}'}{R} \frac{\partial}{\partial t'} I(z', t') \\ + c \frac{\hat{z} \cdot \vec{R}}{R^2} \frac{\partial}{\partial z'} I(z', t') \\ - c^2 \frac{\hat{z} \cdot \vec{R}}{R^3} \lambda(z', t') \end{array} \right] dz' = I(z, t) Z(z, t). \quad (3.9)$$

The accumulated line charge density (positive polarity) in the channel during the return stroke can be evaluated based on the continuity equation:

$$\frac{\partial}{\partial z'} I(z', t') = - \frac{\partial}{\partial t'} \lambda(z', t') \quad (3.10)$$

Where, μ_0 is the permeability and ϵ_0 the permittivity of free space, I is the current and Z the channel resistance per meter. z represents the channel element under consideration and z' the any element along the channel. \hat{z} is the unit vector for z . The \vec{E}^A is the initial longitudinal electric field in the channel, which depends on the cloud and leader sheath charge just before the return stroke:

$$E^A(z) = \begin{cases} E_{DL} & z \in D_{DL} + H' \\ E_{ST} & z \in D_S \\ E_{UL} & z \in D_{UL} \end{cases} \quad (3.11)$$

The integral term in Eq. (3.9) is known as the scattered field, which is represented with E^B hereafter. \vec{R} is the vector distance pointing from z' to z , and $t' = t - R/c$ is the time delay from z' to z . $C(\vec{z})$ represents the whole channel $H + H'$ and its mirror image on ground.

Since the return stroke front is propagating along the previously existing leader channel that is a thin conductive core surrounded by a thick corona sheath with negative charges, parts of the positive charges accumulated on the core by the return stroke current front will diffuse into the corona sheath to neutralize the negative charges there. The positive charge diffusing rate depends on the product of the corona sheath conductivity and radial electric field produced by the positive charges on the core surface. Assume that the line density of positive charges on the core is $\lambda_C(z', t')$ and that diffused into the corona sheath is $\lambda_S(z', t')$, the radial electric field on the core surface will be $\lambda_C(z', t')/\epsilon_0$. If we assign the corona sheath a uniform line conductivity of σ_S , which is taken as $10 \mu\text{S/m}$ in this study [Maslowski and Rakov, 2006], then we have:

$$\lambda(z', t') = \lambda_C(z', t') + \lambda_S(z', t'), \quad (3.12)$$

$$\frac{\partial}{\partial t'} \lambda_C(z', t') = -\frac{\partial}{\partial t'} \lambda_S(z', t') = -\frac{\sigma_S}{\epsilon_0} \lambda_C(z', t'), \quad (3.13)$$

$$r_S(z', t') = [\lambda_L(z') + \lambda_S(z', t')]/[2\pi\epsilon_0 E_C(z')]. \quad (3.14)$$

Where $r_S(z', t')$ represents the changing corona sheath radius derived from Eq. (3.2), and for $z' > H$ it is supposed to be no larger than $r_S(H, t')$.

3.4 Computing Scheme for Return Stroke Modeling

3.4.1 Numerical solution for the current

The channel $H+H' \approx 2H$ is divided into $2N$ number of very small spatial element each with a length of Δs . The evolution time is divided into M number of time step each with an interval of Δt . To achieve good accuracy and adapt to the speed of light c , the spatial element size Δs is related to the time step Δt by $\Delta s = 2c\Delta t$. From Eq. (3.10), taking the current in element i at time step j as $I_{i,j}$, the line density of charges accumulated in element i at step j is given by:

$$\lambda_{i,j} = \lambda_{i,j-1} + \frac{\Delta t}{2\Delta s} (I_{i-1,j-1} - I_{i+1,j-1}) \quad (3.15)$$

Similarly, from Eqs. (11) - (13), the numerical solutions for $\lambda_C(z', t')$, $\lambda_S(z', t')$ and $r_S(z', t')$ for element i at time j are given by:

$$\lambda_{C,i,j} = \lambda_{C,i,j-1} \cdot e^{-\frac{\sigma_S \Delta t}{\epsilon_0}} + \frac{\Delta t}{2\Delta s} (I_{i-1,j-1} - I_{i+1,j-1}). \quad (3.16)$$

$$\lambda_{S,i,j} = \lambda_{S,i,j-1} + \lambda_{C,i,j-1} \cdot \left(1 - e^{-\frac{\sigma_S \Delta t}{\epsilon_0}}\right). \quad (3.17)$$

$$r_{S,i,j} = r_{S,i,0} + \lambda_{S,i,j} / (2\pi\epsilon_0 E_{C,i}). \quad (3.18)$$

Where, $\lambda_{i,0} = \lambda_{C,i,0} = \lambda_{S,i,0} = 0$, and $r_{S,i,j} = r_{S,N,j}$, for $i > N$.

In such, the TD-EFIE equation can be rewritten as:

$$E_i^A - E_{i,j}^B = I_{i,j} Z_{i,j} \quad (3.19)$$

Set $N_{UL} = D_{UL}/\Delta s$, $N_{ST} = D_S/\Delta s$, and $2N = (H+H')/\Delta s$, then

$$E_i^A = \begin{cases} E_{DL} & \text{for } i = N_{UL} + N_{ST} \sim 2N \\ E_{ST} & \text{for } i = N_{UL} \sim N_{UL} + N_{ST} \\ E_{UL} & \text{for } i = 1 \sim N_{UL} \end{cases} \quad (3.20)$$

Taking account of the space integral effect of each element Δs , the integral convergence as well as the charge diffusing effect, $E_{i,j}^B$ can then be written as:

$$\begin{aligned}
E_{i,j}^B &= E_{i,j} + \frac{\mu_0}{4\pi} \sum_{\substack{u=u'=1 \\ u \neq i}}^{2N} \left[\begin{aligned} &+ \frac{I_{u,v} - I_{u,v-1}}{\Delta t} \cdot \ln \left(\frac{|u-i|+0.5}{|u-i|-0.5} \right) \\ &+ \frac{I_{u',v'} - I_{u',v'-1}}{\Delta t} \cdot \ln \left(\frac{u'+i-0.5}{u'+i-1.5} \right) \\ &+ \frac{I_{u+1,v} - I_{u-1,v}}{2\Delta s} \cdot \frac{i-u-0.5}{|i-u-0.5|} \cdot c \cdot \ln \left(\frac{|u-i|+0.5}{|u-i|-0.5} \right) \\ &+ \frac{I_{u'+1,v'} - I_{u'-1,v'}}{2\Delta s} \cdot c \cdot \ln \left(\frac{u'+i-0.5}{u'+i-1.5} \right) \\ &- \frac{\lambda_{C,u,v} + \alpha_{u,v} \lambda_{S,u,w}}{\Delta s} \cdot \frac{i-u}{|i-u|} \cdot c^2 \cdot \frac{1}{(u-i)^2 - 0.25} \\ &+ \frac{\lambda_{C,u',v'} + \alpha_{u',v'} \lambda_{S,u',w'}}{\Delta s} \cdot c^2 \cdot \frac{1}{(u'+i-1)^2 - 0.25} \end{aligned} \right] \\
&= E_{i,j} + E_{i,j}^C \tag{3.21}
\end{aligned}$$

Where, $v = j - 2|u - i|$, $w = j - \text{int}\left(\frac{2|u-i|}{\alpha_{u,v}}\right)$,

$v' = j - 2(i + u' - 1)$, $w' = j - \text{int}\left(\frac{2(i+u'-1)}{\alpha_{u',v'}}\right)$,

$\alpha_{u,v} = \frac{|u-i|}{\sqrt{(u-i)^2 + (r_{S,u,v}/\Delta s)^2}}$, $\alpha_{u',v'} = \frac{|u'+i-1|}{\sqrt{(u'+i-1)^2 + (r_{S,u',v'}/\Delta s)^2}}$,

and i is for the element under consideration, u for any other element and u' for the mirroring element of u . The v is for the time retard of the current and charge on the core of the element u , and v' is for that of the mirroring element u' . The w is for the time retard of the charge diffused into the corona sheath of the element u , and w' is for that of the mirroring element u' . The $\alpha_{u,v}$ is a coefficient for diffused charges in corona sheath of the element u at time v . Due to a uniform dl_{ij}/dz and λ_{ij} are assigned for each element, the contribution from these two terms to each element itself is zero. The E_{ij} represents the scatter field due to dl_{ij}/dt in Eq. (3.9). It takes a

critical role to $I_{i,j}$ and needs to be treated carefully. By introducing a self-induction-like parameter $L_{i,j}$ instead of $E_{i,j}$, the $I_{i,j}$ can be solved based on equations (3.19) & (3.21) as:

$$I_{i,j} = I_{i,j-1} e^{\frac{-\Delta t}{g_{i,j} L_{i,j} + g_{i,j} (E_{i,j}^A - E_{i,j}^C)}} (1 - e^{\frac{-\Delta t}{g_{i,j} L_{i,j}}}). \quad (3.22)$$

Where, $g = 1/Z$ is the conductance. L is the self-induction-like parameter of the element under consideration, which is estimated as:

$$L_{i,j} = \frac{\mu_0}{4\pi} \int_{-\frac{\Delta s}{2}}^{\frac{\Delta s}{2}} \frac{1}{\sqrt{r_{i,j}^2 + z^2}} dz = \frac{\mu_0}{4\pi} \ln \frac{\Delta s}{r_{i,j}}. \quad (3.23)$$

Where, r is the channel core radius which evolves with time. The channel core heating (T - temperature) and expansion (V - volume and P - pressure) may follow a non-linear relationship of $PV \sim nRT$, with the R might be a function of T at high temperature. The core conductivity (σ) depends the product of density (N_e) and mobility (v_e) of electrons. In general, a higher T causes a higher N_e but a lower v_e in ionized gas. There are many studies examining the electric conductivity as a function of the temperature, $\sigma(T)$, for various gases at high temperature. Based on computations [Devoto, 1967] and experiments [Riaby et al., 2010], it is found that the σ increases linearly with T in the range of 6000 ~ 10000 °K in partially ionized argon. Morris et al. (1970) have measured the electric conductivities of Hydrogen, Nitrogen, and Argon at temperatures up to 14000 °K. Their results also show that the σ is linear in T below 5000 °K and has a change in slope at 8000 °K above, for all these gases. Based on above researches and for the first order approximation, we take $PV \sim T$ and $\sigma \sim T$, and assume V and P weight the same against the change of T , then we have $V^2 \sim \sigma$. For a unit length of channel, as $V = \pi r^2$ and $g = \pi r^2 \sigma$, $V^2 \sim \sigma$ means $r^6 \sim g$. As such, the core radius versus the core conductance can be approximated as:

$$\frac{r_{i,j}}{r_0} = \left(\frac{g_{i,j}}{g_0}\right)^{\frac{1}{6}}. \quad (3.24)$$

Where, g_0 is the initial channel conductance which is determined from the Z in Eq. (3.8). r_0 is the initial channel core radius. In this study, $r_0 = 2.5$ mm corresponding to $g_0 = 2$ S/m is referred. Such an approximation may lead to a slower expansion of r versus g than the reality.

3.4.2 Evolution of the channel conductance

For the arcing process within the streamer gap, the evolution of conductance per unit length $g(t)$ and its numerical solution are based on the Toepler's spark law as [Kumar et al., 2008]:

$$g(t) = \frac{\int_0^t I \cdot dt}{C_t}, \quad g_{i,j} = \sum_{j'=1}^j I_{i,j'} \cdot \Delta t \cdot C_t. \quad (3.25)$$

Where C_t is a constant of 0.02 volt-second. Streamer gap channel will transfer into a leader channel when its conductance rises to that of the leader channel.

The variation of conductance per unit length of the leader channel (both DNL and UCL) is based on the first-order arc function as [Rizk, 1989]:

$$\frac{d}{dt} g(t) = \frac{g_{\infty}(I) - g(t)}{\theta}. \quad (3.26)$$

Where, $g_{\infty}(I)$ is the maximum conductance that can be achieved at a steady current I , and θ is a time constant for $g(t)$ to rise/fall to $g_{\infty}(I)$ at steady current condition.

Based on model testing results, we propose:

$$\theta = \begin{cases} \theta_r = 4 \sim 20 \mu s & \text{for current rising stage} \\ \theta_f = 40 \sim 200 \mu s & \text{for current falling stage} \end{cases}$$

We also propose:

$$g_{\infty}(I) = I^{1+\alpha} / C_a. \quad (3.27)$$

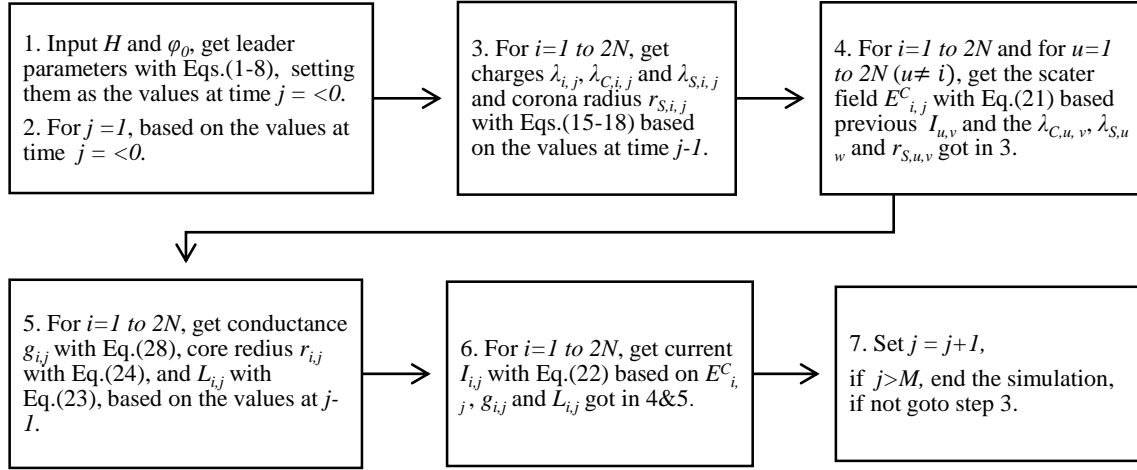


Fig.3.3. Flowchart of the algorithm for modelling of return stroke current.

Where, C_a is a constant of 50000W and α a constant of 0.2~0.4 for cases of large impulsive current (like return stroke). For cases of small steady current (like leader), $C_a = C_b = 30000W$ and $\alpha = 1$, as equation (6). For comparison, *Huzler et al. (1978)* in a leader propagation model proposed $\vartheta_r = 30$ us, $\vartheta_f = 500$ us, and the $\alpha = 0.4$. The numerical solution of equation (26) for the arc regime is then given by:

$$g_{i,j} = g_{i,j-1} e^{-\frac{\Delta t}{\theta}} + g_{\infty}(I_{i,j-1})(1 - e^{-\frac{\Delta t}{\theta}}). \quad (3.28)$$

For easy understanding of the algorithm for modelling of the return stroke current, a flowchart is provided as in **Fig. 3.3**.

3.5 Modeling of Light and Electromagnetic Emissions of Return Stroke

3.5.1 Electrical and Magnetic Fields from Return Stroke

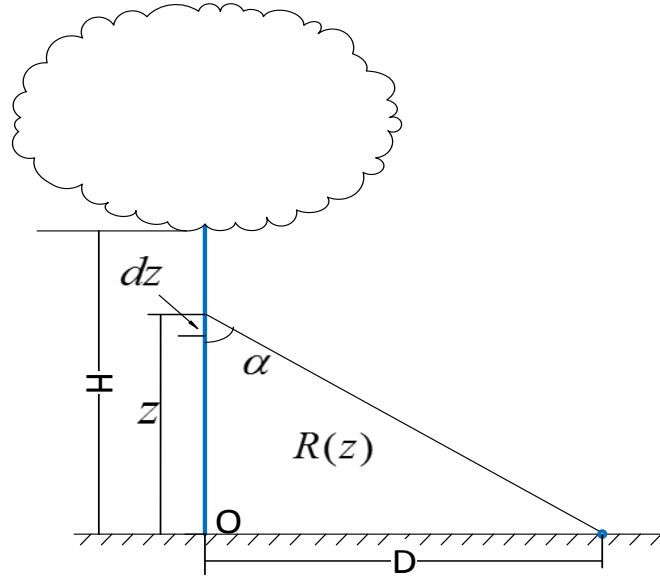


Fig. 3.4. Illustration of calculation of return stroke electromagnetic fields.

As shown by **Fig.3.4**, with the simulated current, the vertical electric field produced by a return stroke on ground can be easily estimated as follows (Cooray, 2014):

$$E_V(D, t) = \left[\begin{array}{l} \frac{1}{2\pi\epsilon_0} \int_0^H \frac{2-3 \sin^2 \alpha(z)}{R^3(z)} \int_0^t I \left(z, \tau - \frac{R(z)}{c} \right) d\tau dz \\ + \frac{1}{2\pi\epsilon_0} \int_0^H \frac{2-3 \sin^2 \alpha(z)}{cR^2(z)} \cdot I \left(z, t - \frac{R(z)}{c} \right) dz \\ - \frac{1}{2\pi\epsilon_0} \int_0^H \frac{\sin^2 \alpha(z)}{c^2 R(z)} \cdot \frac{\partial}{\partial t} I \left(z, t - \frac{R(z)}{c} \right) dz \end{array} \right]. \quad (3.29)$$

$$\sin \alpha(z) = \frac{D}{\sqrt{D^2+z^2}}, \quad R(z) = \sqrt{D^2 + z^2}.$$

Where, $E_V(D, t)$ is the vertical electric field at point of P on ground. D is the distance from observation point P on ground to the lightning channel base.

The corresponding numerical solution is:

$$E_V(D, j) = \frac{\Delta s}{2\pi\epsilon_0} \sum_{i=1}^N \left[\begin{array}{c} \frac{2-3 \sin \alpha_i^2}{R_i^3} \sum_{j'}^j I \left(i, j' - \frac{R_i}{c} \right) \\ + \frac{2-3 \sin \alpha_i^2}{cR_i^2} I \left(i, j - \frac{R_i}{c} \right) \\ - \frac{\sin \alpha_i^2}{c^2 R_i \Delta t} \left(I \left(i, j - \frac{R_i}{c} \right) - I \left(i, j - \frac{R_i}{c} - 1 \right) \right) \end{array} \right]. \quad (3.30)$$

Similarly, the horizontal magnetic field at point P on ground is given by [Cooray, 2014]:

$$B_\phi(D, t) = \frac{1}{2\pi\epsilon_0 c^2} \int_0^H \left(\begin{array}{c} \frac{\sin \alpha(z)}{R^2(z)} I \left(z, t - \frac{R(z)}{c} \right) \\ + \frac{\sin \alpha(z)}{cR(z)} \frac{\partial}{\partial t} I \left(z, t - \frac{R(z)}{c} \right) \end{array} \right) dz. \quad (3.31)$$

The corresponding numerical solution is:

$$B_\phi(D, j) = \frac{1}{2\pi\epsilon_0 c^2} \sum_{i=1}^N \left[\begin{array}{c} \frac{\sin \alpha_i}{R_i^2} I \left(i, j - \frac{R_i}{c} \right) + \\ \frac{\sin \alpha_i}{cR_i \Delta t} \left(I \left(i, j - \frac{R_i}{c} \right) - I \left(i, j - \frac{R_i}{c} - 1 \right) \right) \end{array} \right]. \quad (3.32)$$

3.5.2 Light Emission from Return stroke

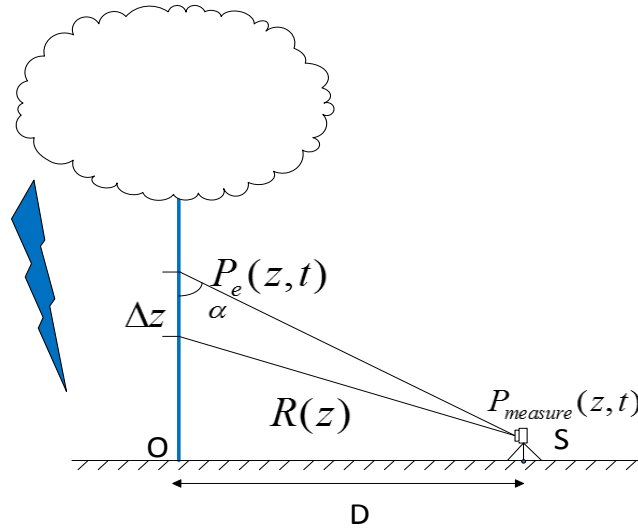


Fig. 3.5. Illustration of calculation of return stroke light emissions.

According to energy conservation law, all energy that consumed by light, thunder, electromagnetic wave and heating is from the input electric energy. The input electric power per unit length of channel segment is given by:

$$P_e(z, t) = I(z, t)^2 / g(z, t). \quad (3.33)$$

Researches show that about 10% of the electric power is released by light emission [Guo et al., 1983; Quick and Krider, 2013]. We assume that at any moment the power related to the channel heating and lighting is a fraction (C_l) of the total electric power as $C_l P_e$ and the lighting power is P_l . As such, the instant net power for channel heating is $C_l P_e - P_l$ and the channel accumulated heating energy will be $W_h = \int (C_l P_e - P_l) dt$. Physically, the light radiation power depends on the volume (or mass: Δm) fraction of air excited and the level of excitation (temperature: T) during the return stroke, i.e. $P_l \sim T \Delta m$, [Ma et al., 2011]. The channel rising temperature in turn depends on the accumulated heating energy and the heated mass, i.e. $W_h \sim (T - T_0) \Delta m$, where T_0 is the initial gas temperature. As such, the lighting power could be supposed to be proportional to the channel accumulated heating energy, i.e. $P_l(z, t) \sim W_h(z, t)$. Meanwhile, the light emission may make the channel cooling down after a certain time (θ_l) if the channel accumulated heating energy keeps no change. As such, the lighting power per unit length of channel can be related to the total input electric power as:

$$P_l(z, t) = \frac{1}{\theta_l} \int_0^t (C_l P_e(z, \tau) - P_l(z, \tau)) d\tau. \quad (3.34)$$

Where, C_l is a numerical constant representing the percentage of the input electric power related to the channel heating and lighting, and θ_l is a time constant reflecting the channel cooling down rate due to light emission, which is taken as the same as the θ_f in this study. The solution of equation (3.34) is:

$$P_l(z, t) = \frac{c_l}{\theta_l} e^{-\frac{t}{\theta_l}} \int_0^t P_e(z, \tau) e^{\frac{\tau}{\theta_l}} d\tau. \quad (3.35)$$

Assuming the light source is isotropic (**Fig.3.5**), for a light sensor at point S with an exposure time ΔT and a channel section view of $z \sim z+\Delta z$, the light power at the sensor per unit area is:

$$P_m(D, z, t) = \frac{1}{\Delta T \Delta z} \int_z^{z+\Delta z} \int_{t-\Delta T}^t \frac{\sin \alpha(z')}{4\pi R(z')^2} P_l(z', \tau - \frac{R(z')}{c}) d\tau dz'. \quad (3.36)$$

Chapter 4. Simulation Results and Comparison with Observations

Table 1. Initial parameters for leader-return stroke modeling

Symbol	Quantity	Value
E_{c0}	Critical negative electric field at ground (Eq.3.4)	-750 kV/m
E_{c0+}	Critical positive electric field at ground (Eq.3.4)	+500 kV/m
C_b	Leader power constant (Eq.3.6)	30000 W/m
C_t	Streamer heating up constant (Eq.3.25)	0.02 V-Sec.
ϑ_r	Time constant for rising conductance (Eq.3.26)	5 μ s
ϑ_f	Time constant for falling conductance (Eq.3.26)	50 μ s
C_a	Return stroke power constant (Eq.3.27)	50000 W/m
α	Power index for large current for Eq.3.27	0.2
C_l	Coefficient of energy for lighting (Eq.3.34)	0.1
ϑ_l	Time constant for lighting (Eq.3.34)	50 μ s
r_0	Initial reference channel radius (Eq.3.24)	2.5 mm
g_0	Initial reference channel conductance (Eq.3.24)	2 S/m
Δs	Channel segment length for computing	2.4 m
Δt	Time step interval for computing	4 ns
ϵ_0	Free space permittivity ($C^2/m^2/N$)	8.86×10^{-12}
μ_0	Free space permeability (H/m)	$4\pi \times 10^{-7}$
σ_s	Line conductivity of corona sheath (Eq.3.13)	10 μ S/m

With the present model and the initial values in **Table 1**, we have studied the evolution of the current and the light and electromagnetic emissions of a leader-return stroke with different initiation potentials (φ_0). There are totally 14 cases studied, with φ_0 ranges from -10 ~ -140 MV in an interval of -10 MV. **Table 2** shows the leader parameters (initial values of return stroke channels) corresponding to the 14 cases, which are calculated with the leader model in Section 3.2 and the initial values in **Table 1**.

The channel height ($H+H'$) is determined in a way that the return stroke current decays to about zero when it arrives at the upper end of the channel. The current of UCL is set to $0.3I_{DL}$ and that of the streamer gap is set to vary from I_{DL} when at DNL tip down to $0.3I_{DL}$ when at UCL tip. The streamer resistance shown in the table is for that when the streamer current equals I_{DL} for reference purpose. As can be seen from the table, the higher of the initiation potential, the longer of the lightning channel and the streamer gap as well as the UCL, and the larger of the leader current. With the return stroke model in Section 3.3 and the leader parameters in **Table 2**, simulations of the return stroke parameters for the 14 cases have been done. Since the property of return stroke parameters for all the 14 cases are similar to each other, in following, we take the case $\varphi_0 = -50$ MV as an example to illustrate details of the property of return stroke parameters.

Table 2. The modeled later stage leader parameters with different cloud initiation potentials.

Cloud potential φ_0 (MV)	Channel height H (m)	Streamer gap D_s (m)	UCL Length D_{UL} (m)	DNL E-field E_{DL} (V/m)	UCL E-field E_{UL} (V/m)	DNL resistance Z_{DL} (Ω /m)	UCL resistance Z_{UL} (Ω /m)	Streamer resistance Z_{ST} (Ω /m)	DNL current I_{DL} (A)	DNL core radius r_0 (mm)
-10	300	9.6	2.4	7816	23955	1721	19129	179665	4.17	0.64
-20	1200	21.6	4.8	2537	8458	214	2385	63433	11.8	0.91
-30	2400	36	7.2	1380	4600	63.5	705	34500	21.7	1.12
-40	3600	48	12	895	2986	26.7	294	22396	33.5	1.28
-50	4800	62.4	14.4	640	2136	13.6	152	16018	46.8	1.44
-60	6000	76.8	16.8	487	1624	7.9	88	12180	61.6	1.58
-70	7200	88.8	21.6	386	1288	5	55.3	9663	77.6	1.70
-80	9000	103.2	24	316	1054	3.3	37.5	7907	94.8	1.83
-90	9600	115.2	28.8	265	883	2.3	26	6625	113	1.94
-100	12600	129.6	31.2	226	754	1.7	19	5655	132.6	2.04
-110	14400	144	33.6	196	653	1.3	14.2	4901	153	2.13
-120	16200	156	38.4	172	573	1	11	4300	174.4	2.22
-130	18000	170.4	40.8	152	508	0.78	8.6	3813	196.7	2.32
-140	19600	182.4	45.6	137	455	0.62	6.9	3412	219.8	2.42

4.1 Return Stroke Current and Conductance

Shown in **Fig. 4.1** are the variations of current, channel conductance, channel core radius and the charge accumulation with time and height for the return stroke of case $\varphi_0 = -50$ MV. The initial channel condition is: the channel length $H = 4800$ m, UCL length $D_{UL} = 14.4$ m, streamer gap $D_{ST} = 62.4$ m, DNL current $I_{DL} = 46.8$ A, and DNL core radius $r_0 = 1.44$ mm.

As shown in the figure, the initial negative charge (λ_L in Eq. (3.1)) in the leader corona sheath shows firstly an increase from the zero when at the ground level to its maximum of about -0.65 mC/m when near the connecting point (about 77 m high), and then a decrease to about -0.18 mC/m when at 4.8 km high. Similarly, the positive charge (λ in Eq. (3.12)) accumulated along the channel by the return stroke shows firstly an increase from the zero when at the ground level to its maximum of about $+0.35$ mC/m when near the connecting point, and then a decrease to about $+0.18$ mC/m when at 4.8 km high. The diffusing current peak also shows firstly an increase from the zero when at ground level to its maximum of about 235 A/m when near the connecting point, and then a decrease to about 17 A/m when at 4.8 km high.

Table 3 is a statistics of the current waveform, return stroke speed and channel conductance along the channel for this case. Both the current amplitude and its propagation speed decrease exponentially while the current waveform becomes

flatter and wider, with the increase of the height. The current peak (I_p) is 60 kA when near ground and decreases to 9 kA when at 4.8 km high. The return stroke speed (v_r), which is measured using the 50% peak of the current wave, is 2.0×10^8 m/s when near ground and decreases to 1.1×10^8 m/s when at 4.8 km high, which is within the range of observed return stroke speed in the literature. The current waveform has a 10% to 90% rising time (T_r) of $0.3 \mu\text{s}$ when near ground and $4.9 \mu\text{s}$ when at 4.8 km high. The full width at half maximum (FWHM) is $8.5 \mu\text{s}$ when near ground and $53.7 \mu\text{s}$ when at 4.8 km high. The channel core expands from the initial 1.4 mm to 2.9 mm in radius. The amplitude of both the channel conductance and core radius decreases exponentially while their waveform becomes flatter and wider, with the increase of the height. Especially, *Shao and Jacobson (2012)* studied the behavior of return stroke current based on the remotely detected electric field change waveform. Their results showed that the return stroke current traveled in a dispersive and lossy manner, which are well consistent with the present results.

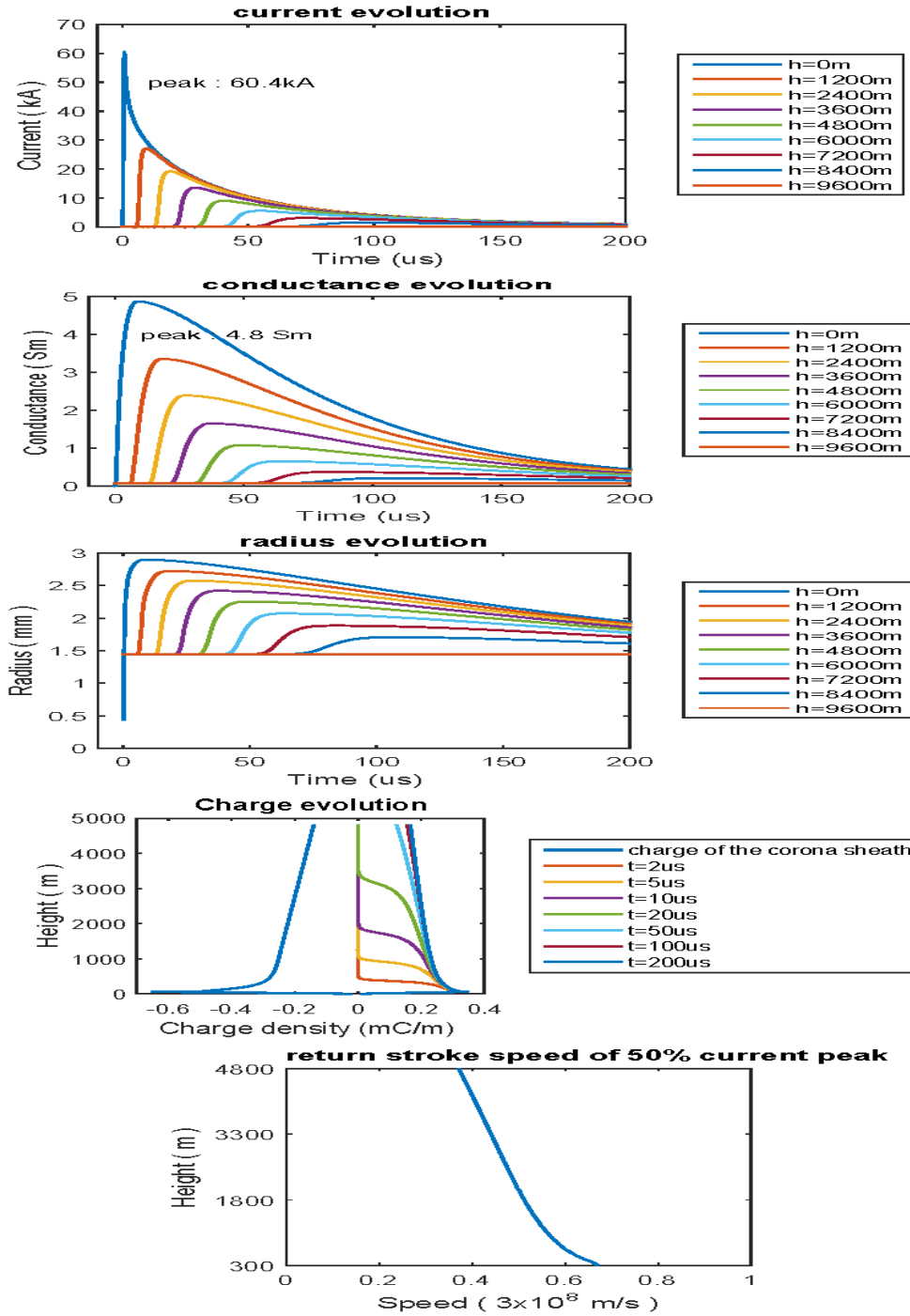


Fig. 4.1. The spatial and temporal evolution of the return stroke current, channel conductance, core radius, the charge deposit and the return stroke speed for the return stroke for case $\phi_0 = -50$ MV.

Fig. 4.2 is an expansion of the current in **Fig. 4.1**, but focuses on the rising front of the current along the channel below 150 m, where the attachment process occurs. As shown in the figure, the current front firstly appears at $h=45.6$ m where is the middle of the streamer gap and then moves in two directions. One wave moves upward from $h=45.6$ m (middle of streamer gap) to $h=60$ m, then $h=76.8$ m (tip of DNL) and then $h=91.2$ m, with an average speed of 0.5 speed of light. One wave moves downward from $h=45.6$ m to 31.2 m, then $h=14.4$ m (tip of UCL) and then $h=0$ m, with an average speed of 0.4 speed of light. As the downward wave reaches the ground, it is reflected to move upward with a speed of 0.68 speed of light and its amplitude is doubled. Such a two-current wave attachment process is well consistent with the observations by *Wang et al. (2014)*.

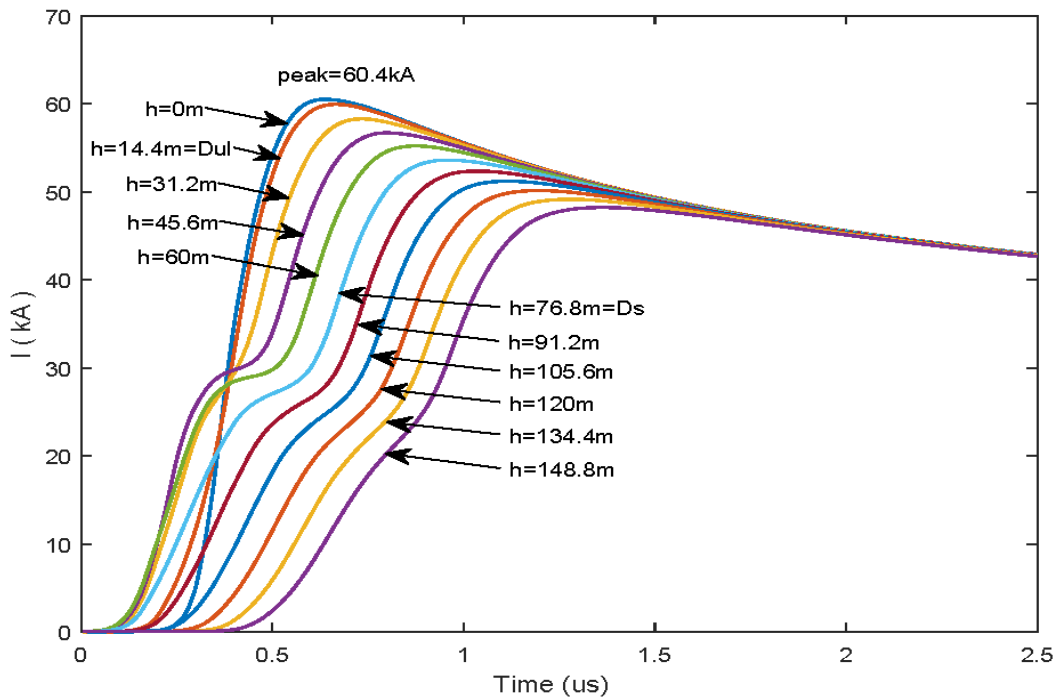


Fig.4.2. The rising front of the current along the channel below 150m where the attachment occurs, expanded from **Fig. 4.1**, for case $\phi_0 = -50$ MV.

Table 3. Statistics of modelled current and speed and channel conductance for the return stroke for case $\varphi_0 = -50$ MV.

Channel altitude z (m)	Rising front T_r (us)	Full wave width $FWHM$ (us)	Current peak I_p (kA)	Return speed v_r/c	Conduct. peak g_p (Sm)	Core peak radius r_p (mm)
0	0.31	8.49	60.42	-	4.83	2.90
60	0.46	10.91	55.26	0.68	4.78	2.87
600	0.79	25.70	33.90	0.61	3.98	2.80
1200	1.49	31.40	27.09	0.55	3.34	2.72
1800	2.09	34.93	22.74	0.51	2.83	2.65
2400	2.61	37.95	19.25	0.48	2.38	2.57
3000	3.09	41.01	16.25	0.45	1.99	2.50
3600	3.60	44.44	13.59	0.43	1.64	2.42
4200	4.18	48.54	11.21	0.40	1.34	2.34
4800	4.88	53.72	9.08	0.37	1.07	2.25

4.2 Electrical and Magnetic Fields from Return Stroke

Fig. 4.3 shows the calculated electrical and magnetic fields at different distances on ground, for the return stroke of case $\varphi_0 = -50$ MV. The calculation is based on the current shown in **Fig. 4.1** with the model in Section 3.5. It should be pointed out that there is a little difference in the electromagnetic field calculated when only the lower half channel H is considered with that when the whole channel $H+H'$ is considered. It is noted that at a distance less than 1000 m the waveform of the magnetic field is quite similar to that of the channel base current. This implies that we may sense the return stroke current with magnetic field measurements at a close distance. The properties of waveform of modeled electrical and magnetic fields versus distance are well consistent with those in the literature.

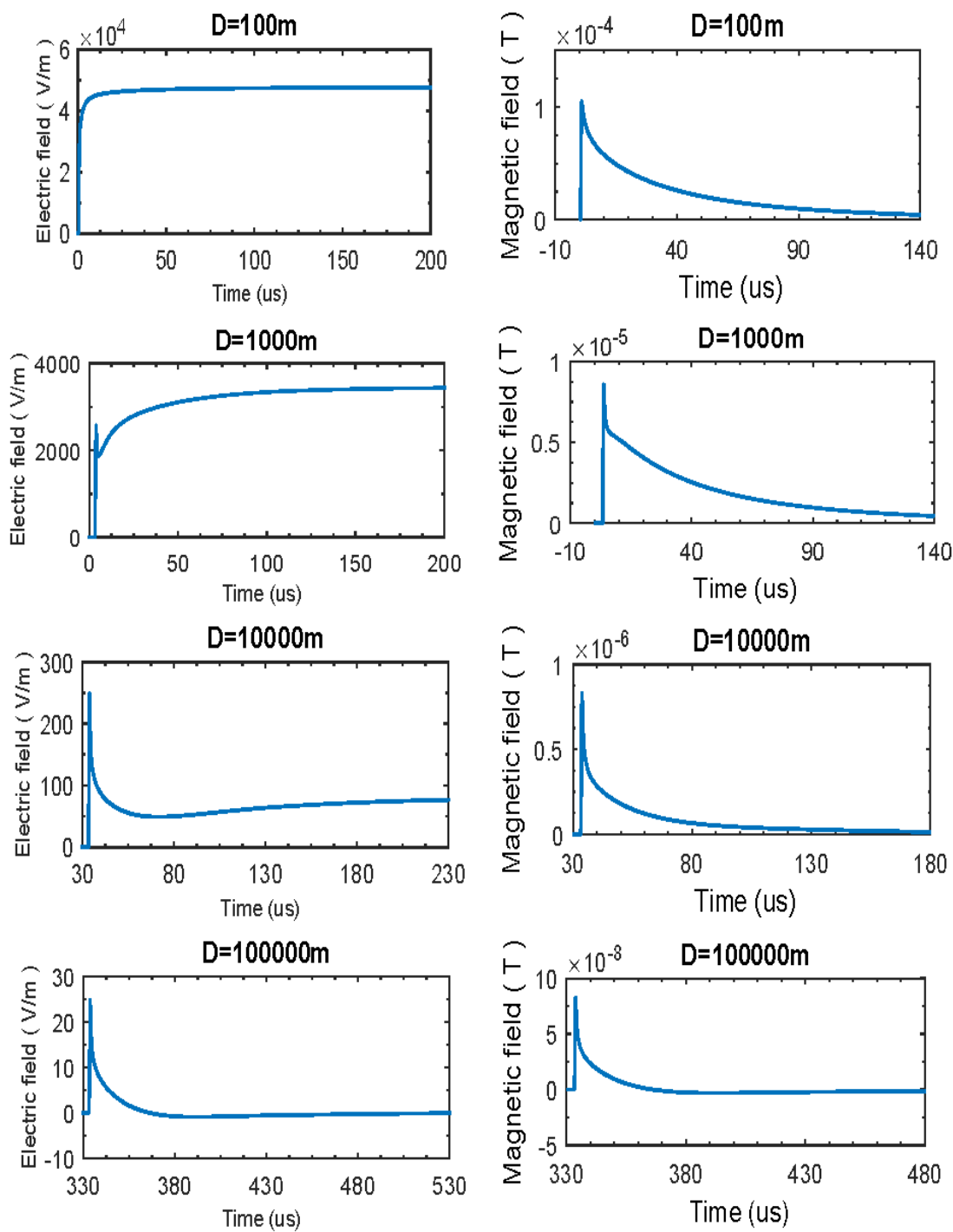


Fig. 4.3. The calculated electrical (left) and magnetic (right) fields at different distance on ground, for the return stroke for case $\phi_0 = -50$ MV.

4.3 Light Emissions from Return stroke

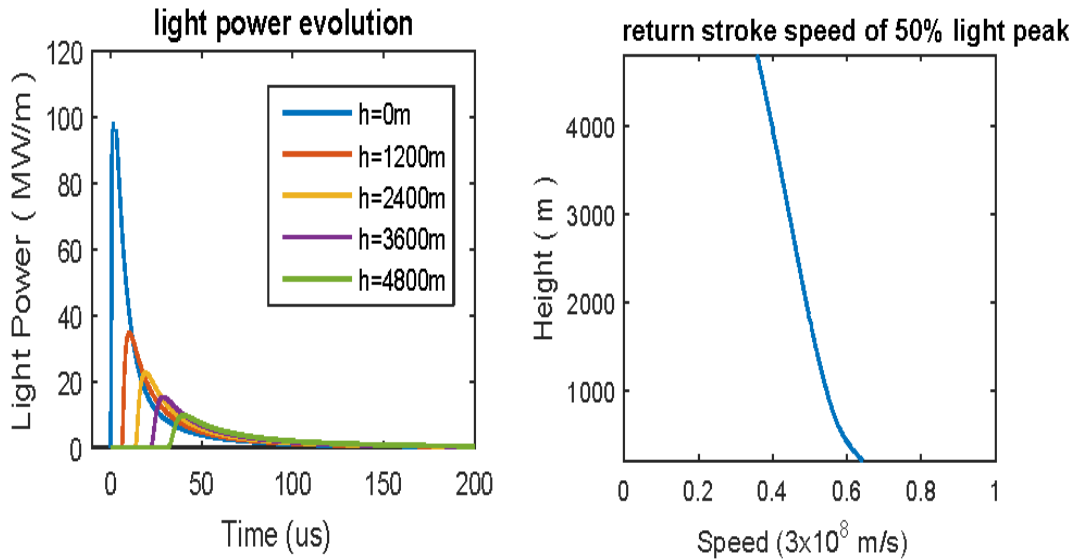


Fig.4.4. Calculated light power per unit channel length versus time and height (left), and the return speed based on the light waveform (right) for the return stroke for case $\phi_0 = -50$ MV.

Fig. 4.4 shows the modeled light power per unit channel length (left) and the return stroke speed based on light power (right) versus the height respectively, for the return stroke of case $\phi_0 = -50$ MV. The calculation is based on the current and conductance shown in **Fig. 4.1** with equation (35) in Section 3.2. The light power peak is 99.1 MW/m when at the channel base and decays sharply to 9.6 MW/m when at 4.8 km high, which are comparable to the estimates of *Guo and Krider (1983)* and *Quick and Krider (2013)*. The return stroke speed here is determined based on the median of the rising front of the light power waveform, which is very like that determined based on the current waveform as shown in **Fig. 4.1**. The return

stroke speed has a trend of decreasing as it propagates upward, which is consistent with the observation results of triggered lightning by *Wang et al. (1999)*.

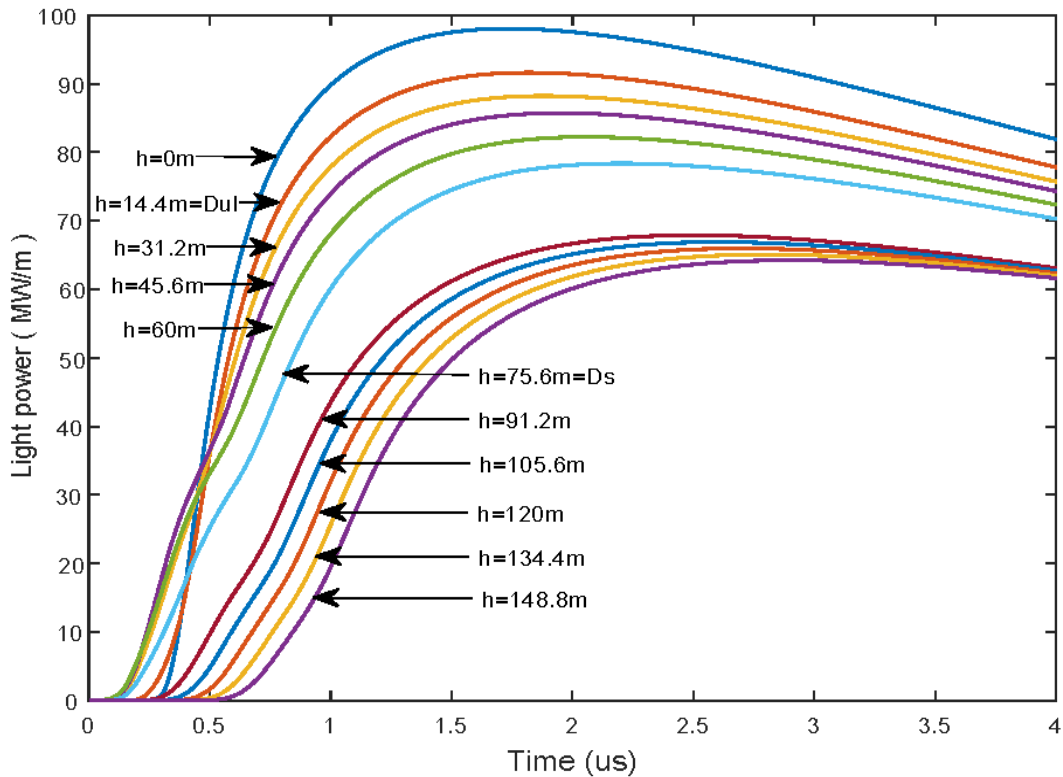


Fig.4.5. Exapasion of the rising front of light power in **Fig. 4.4** for the channel below 150m where the attachment process occurs, for case $\phi_0 = -50$ MV.

Fig. 4.5 is an expansion of the rising front of the calculated light power in **Fig. 4.4**, but focuses on the height below 150 m, where the attachment process is supposed to occur. Similar to the current rising front shown in **Fig. 4.2**, the rising front of the light power also starts with 2 light waves. One light wave moves upward from $h=45.6$ m (middle of the streamer gap) to $h=76.8$ m (tip of DNL) and then $h=91.2$ m, at about 0.5 speed of light. One light wave moves downward from $h=45.6$ m to $h=14.4$ m (tip of UCL) and then $h=0$ m (the ground), at about 0.4 speed of light. The

downward wave reflects at ground and goes upward at 0.65 speed of light. These results are well consistent with the observed attachment processes in triggered lightning discharge by Wang et al. (2014).

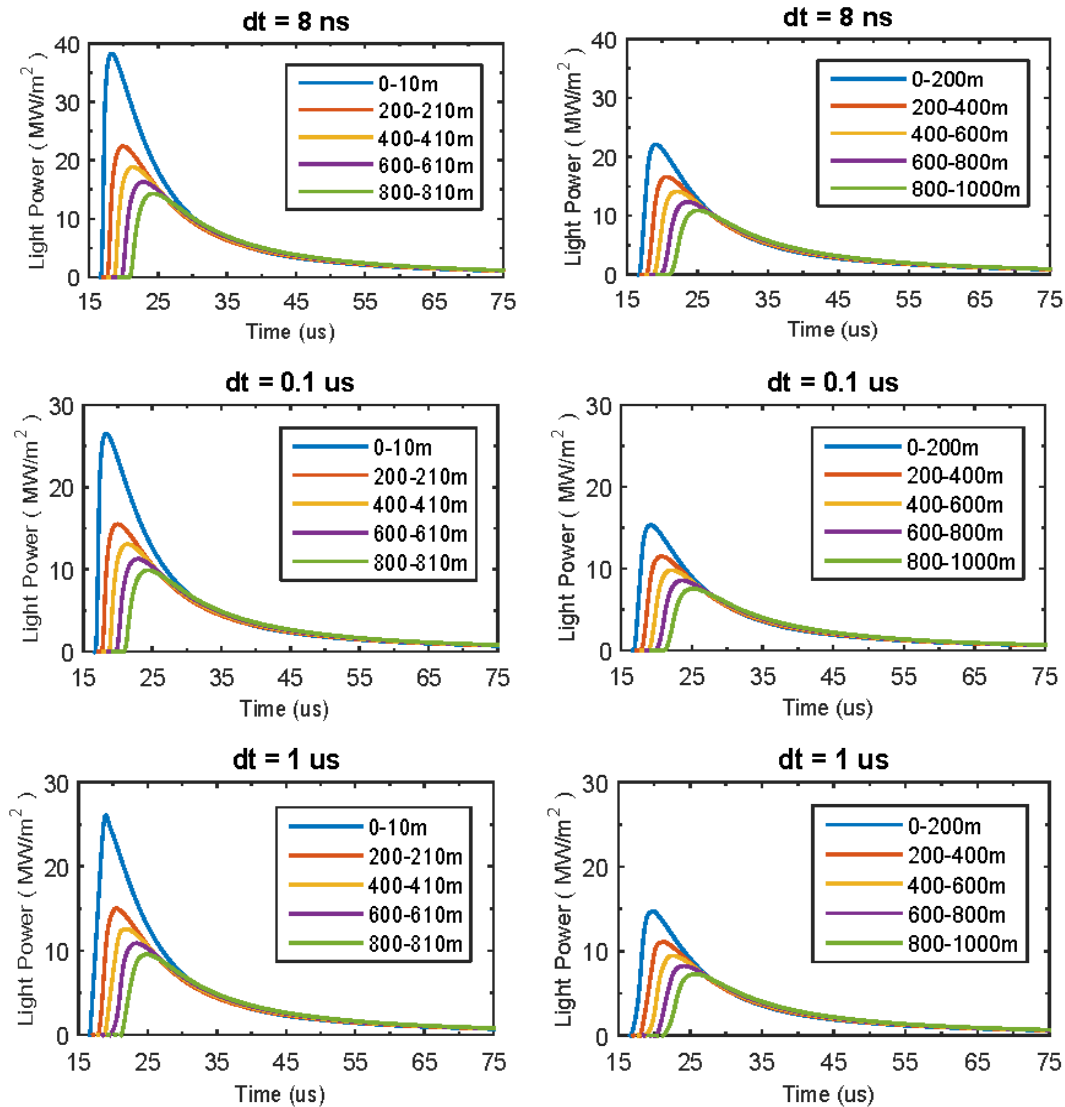


Fig.4.6. Calculated light power per unit area at a sensor with different exposure times (ΔT) and space views (Δz) at a distance of $D = 5$ km on ground, for the return stroke of case $\phi_0 = -50$ MV.

Fig. 4.6 shows the modeled light power detected by a sensor with unit area at 5 km to the channel base on ground with different time and space revolutions, for the return stroke of case $\varphi_0 = -50$ MV. The calculation is based on the light power in **Fig. 4.4** with equation (36) in Section 3.5. It is obvious that the light waveform detected by a sensor varies with the sensor time and space resolutions. The longer the exposure time of the sensor, the wider the light waveform it detected. And also the longer the channel segment viewed by the sensor, the wider the light waveform it detected. These results can well explain those observed light waveforms of return strokes in literature [*Wang et al., 2005; Zhou et al, 2014*].

Shown in **Fig. 4.7** is a comparison of the light waveform at a sensor with an exposure time $\Delta T = 8$ ns and a channel view $\Delta z = 10$ m and 200 m respectively, with the current waveform, for the height of $z = 200$ m, for case $\phi_0 = -50$ MV. It shows that the rising front of light waveform is slower than that of the current, even the exposure time and the space view of the sensor are very small. The larger the space view and exposure time, the slower the rising front of the light waveform than that of the current.

Wang et al. (2005) and *Zhou et el. (2014)* compared the current and optical signal with a high speed detection system for triggered lightning discharges. They found that the rising front of the current is always faster than that of the optical signal, which are well consisten with our simulation results.

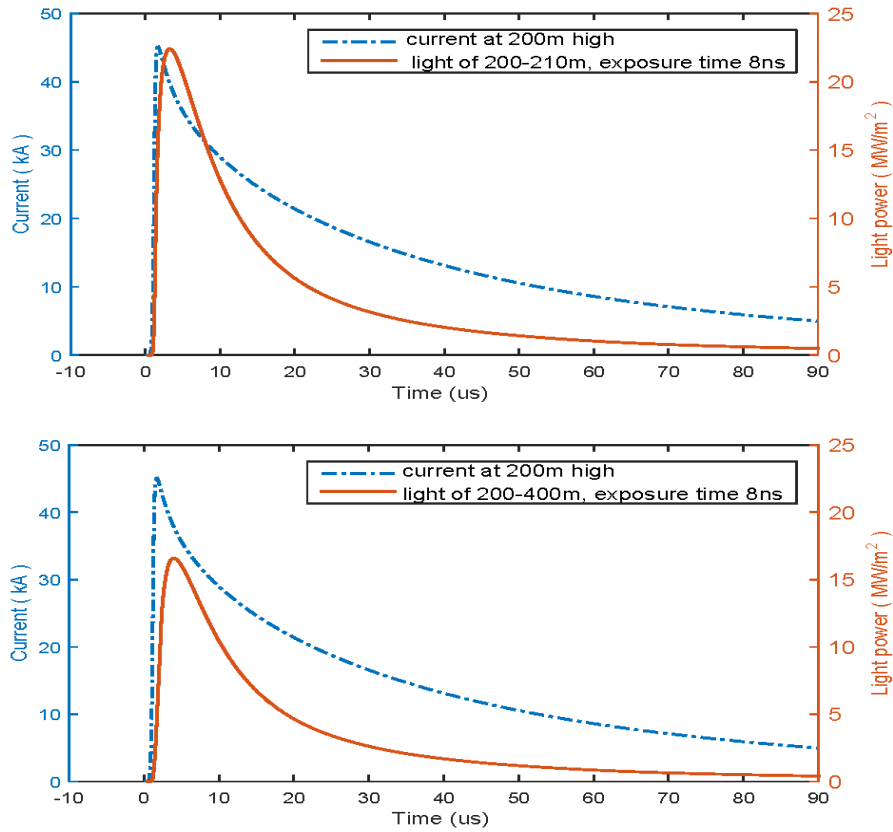


Fig.4.7. Comparisons of the light waveform of a sensor at exposure time $\Delta T=8$ ns and channel view $\Delta z=200\sim 210$ m (upper) and $200\sim 400$ m (lower) respectively, with the current waveform at the channel height $z=200$ m, for the return stroke for case $\varphi_0 = -50$ MV.

Table 4. Summary of modeled return stroke parameters corresponding to different cloud initiation potentials

φ_0 (MV)	I_p (kA)	v_r (3×10^8 m/s)	g_p (Sm)	r_p (mm)	E_{p100} (V/m)	B_{p100} (10^{-9} T)	P_{lp} (MW/m)
-10	2.6~0.3	0.21~0.00	0.05~0.017	1.35~1.13	0.56	1.9	4.76~0.58
-20	10.2~0.8	0.31~0.04	0.35~0.057	1.87~1.38	2.61	8.7	22.4~1.24
-30	23.8~1.7	0.50~0.15	1.15~0.16	2.28~1.64	7.13	23.8	48.7~2.23
-40	41.8~4.5	0.63~0.26	2.70~0.47	2.63~1.96	15.4	51.3	79.3~5.28
-50	60.4~9.1	0.68~0.37	4.86~1.07	2.90~2.25	24.8	82.7	99.1~9.62
-60	76.1~13.4	0.74~0.44	7.00~1.73	3.08~2.44	33.3	111	128~12.9
-70	94.4~20.2	0.77~0.53	9.70~2.85	3.25~2.65	43.3	144	150~17.9
-80	109.5~23.5	0.80~0.58	12.2~3.52	3.38~2.75	51.8	173	167~19.0
-90	127.3~28.9	0.81~0.60	15.3~4.60	3.51~2.87	61.7	206	185~21.7
-100	142.1~32.7	0.82~0.64	18.1~5.47	3.61~2.96	70.7	234	199~22.8
-110	159.6~38.5	0.84~0.69	21.5~6.78	3.71~3.06	79.8	266	213~25.3
-120	177.0~44.5	0.85~0.71	25.0~8.20	3.81~3.16	88.3	298	227~27.7
-130	191.5~48.9	0.85~0.74	28.0~9.37	3.88~3.23	97.4	324	237~28.7
-140	209.0~55.1	0.86~0.76	31.7~11.0	3.96~3.32	106.7	356	248~30.9

Table 4 is a summary of the current peak (I_p), return stroke speed (v_r), conductance peak (g_p) and light power density peak (P_{lp}) along the channel up (z), and the electrical (E_{p100}) and magnetic (B_{p100}) field peaks at 100 km, for all the 14 cases. The first figure in columns 2-4 & 7 is the value at ground level and the second one is that at the upper end of channel H . In overall, the larger the initiation potential φ_0 is, the larger the H , I_p and v_r . For example, $\varphi_0 = -10$ MV corresponds to $H = 300$ m, $I_p = 2.6$ kA and $v_r = 0.21c$ (at channel base), while $\varphi_0 = -140$ MV corresponds to $H = 19.8$ km, $I_p = 209$ kA and $v_r = 0.86c$. The case 2.6 kA might be about the smallest return stroke available in a thunderstorm on earth, while the case 209 kA might be about the strongest one. For each case, all the I_p , v_r , g_p and P_{lp} show an exponentially decreasing trend with the increase of the height.

Chapter 5. Preliminary Study of Lightning Light Spectra for Possible Model Validation

Current propagation and conductivity evolution are the most important two parameters in the return stroke model. Though the two variables cannot be measured or indicated by light change directly, they can be achieved by analyzing data of light propagation.

5.1 Method for Estimation of Channel Temperature from Light Spectra

Light emitting of lightning flash is kind of plasma radiation. There are four kinds of electromagnetic radiation of plasma, excitation radiation, recombination radiation, Bremsstrahlung and cyclotron radiation. Excitation radiation or line radiation is some discrete spectral lines and produced by electron transition between different energy levels of plasma particles. Recombination radiation is continues spectrum and generated by captured free electrons. In weakly ionized plasma with low temperature, excitation radiation or discontinues radiation plays a major role. As temperature rises, continues radiation gradually increases. The last two radiations occur under higher temperature and the wavelength is much shorter than ultra violet light, such as thermonuclear plasma. Therefore, visible light of return stroke mainly consist of line radiation and recombination radiation [*Chen and Trivelpiece, 1976*].

5.1.1. Line spectra of lightning

Excitation radiation or line radiation from lightning has been measured with wavelength range of 286nm ~ 1000nm. Light that shorter than 286nm is on Hartley absorption band and is hard to detect. Most important spectra line is NI, NII, OI, OII and other atomic spectrums [*Wallace, 1964*].

a) Spectrums of neutral nitrogen atom is visible light and near-infrared light, and excitation energy is about 11eV ~13eV. Relatively strong lines are 4223NI(5), 6482NI(21), 8223NI(2), 8629NI(8), 8683NI(1) and so on. The numbers ahead are wavelength of the line, in unit of Å. And the Rome numbers present ion states of the particle. For example, I means neutral atoms, II means single ionization atoms, III means double ionization atoms, and so on. Arabic numerals in parentheses is the number of atomic spectrum multiplets.

b) Single ionized nitrogen atoms generally radiate visible light and violet light with exciting energy from 20eV ~ 30eV. Relatively strong lines are 3330NII(22), 3437NII(13), 3919NII(17), 3995NII(12), 4447NII(15), 4630NII(5), 5001NII(19), 5680NII(3), and so on.

c) Neutral oxygen atoms mainly radiate visible and infrared light with energy level of 10eV ~ 16eV. And relatively strong lines are 7774OI(1), 7947 OI(30), 8447 OI(4), and so on.

d) Single ionized oxygen atoms generally radiate visible light and violet light with exciting energy from 25eV ~ 27eV. And strong spectra lines from them are

3727OII(3), 3749 OII(3), 4075 OII(10) and so on. Spectra band and multiplet of N_2 , N_2^+ , O_2 , NO, Ar, C, OH, NH, CN, H_α , H_β , etc. are also detected from lightning emission. However, nitrogen atom spectra and H_α are often used to determine temperature of the lightning channel [Orville, 1968]. And peak temperature of it is about 2800 ~ 3100 K.

5.1.2. Temperature dependence of spectra lines

Temperature is the characterization of particle average Kinect energy and therefore a statistical average value. During a transient process such as lightning return stroke, temperature of different particles do not reach the equilibrium state. However, research indicates that electrons will reach thermal equilibrium with them within 1 microsecond.

Under the assumption of thermal equilibrium, the atomic energy levels with the same ionization state are populated due to Boltzmann's law:

$$N_n = N_0 \frac{g_n}{g_0} e^{-\frac{E_n}{kT}}. \quad (5.1)$$

Where N_n is the number of atoms in energy level of n , and N_0 is the number of atoms in ground state. E_n is the excitation potential of the level. g is the statistical weight or degeneracy of the corresponding state and is derived from related angular quantum number J .

$$g = 2J + 1. \quad (5.2)$$

The discontinuous spectra lines whether absorption or emission is from transition of atomic energy levels. The intensity of an emission line due to transition s from

level n down to level r is

$$I_{nr} = N_n A_{nr} h \nu_{nr}. \quad (5.3)$$

Where A_{nr} is the Einstein emission coefficient, ν_{nr} is the frequency of emitted photon, and h is Plank's constant. Then the ratio of intensity of two emission lines is

$$\frac{I_{nr}}{I_{mp}} = \frac{g_n A_{nr} \nu_{nr}}{g_m A_{mp} \nu_{mp}} e^{\frac{E_m - E_n}{kT}}. \quad (5.4)$$

Where A is proportional to f/λ^2 , where f is the corresponding oscillator strength and λ is the wave length. And f of NII has been published in 1963 by Melvin L. Prueitt. Therefore the ratio can be derived as

$$\frac{I_{nr}}{I_{mp}} = \frac{g_n \lambda_{mp}^3 f_{nr}}{g_m \lambda_{nr}^3 f_{mp}} e^{\frac{E_m - E_n}{kT}}. \quad (5.5)$$

Then the temperature can be expressed as [Prueitt, 1963]

$$T = \frac{E_m - E_n}{k \ln(I_{nr} g_m \lambda_{nr}^3 f_{mp} / I_{mp} g_n \lambda_{mp}^3 f_{nr})}. \quad (5.6)$$

With this method above, the resulting temperatures are scattered. If enough numbers of spectra lines can be obtained, a reliable average of temperature can be derived. At the temperature of 2000K, nitrogen is singly ionized and therefore, transitions of NII monitors the average temperature of the gas.

5.1.3 Temperature dependence of electrical conductivity

Theoretical relationship between electrical conductivity and temperature may be expressed as [Olsen, 1959]

$$\sigma = e^2 n_e \lambda_e / (3m_e kT)^{1/2}. \quad (5.7)$$

Where n_e is the number density of electron as a function of T and can be calculated with plasma composition. λ_e is electron mean free path and is given by

$$\lambda_e = 1/(n_0 a_0 + \sum n_i a_i). \quad (5.8)$$

Where n_0 and n_i are number density of neutral atom and i -fold ions. a_0 and a_i are cross sections for collisions of electron and heavy particles.

$$a_i = \pi r_i^2 \quad (5.9)$$

r is the gas kinetic atomic radius neglecting the Ramsauer effect.

The electron number density can be derived with Saha equation [Inan and Gołkowski, 2011]

$$\frac{n_i}{n_0} = 2.405 \times 10^{21} \frac{T^{3/2}}{N_i} e^{-\frac{E_i}{kT}} \quad (5.10)$$

Therefore,

$$n_e = \sum i \times n_i \quad (5.11)$$

Considering motions of ions,

$$\sigma = \frac{e^2 n_e \lambda_e}{(3m_e kT)^{1/2}} + \sum \frac{q_i^2 n_i \lambda_i}{(3m_i kT)^{1/2}}. \quad (5.12)$$

Where q_i is the charge of the ion, and λ_i is its mean free path.

The number density of nitrogen and oxygen in the air is known. During the transient process of lightning return stroke, the inner pressure of the channel can be assumed to stay still. Another assumption is that all the gas molecules dissociated into isolated atoms. Given n_0 of nitrogen and oxygen and temperature, n_e can be calculated and therefore the conductivity σ .

5.2 Light spectrum of lightning return strokes

5.2.1 Existing data from America

Following is an example of natural lightning return stroke recorded in America,

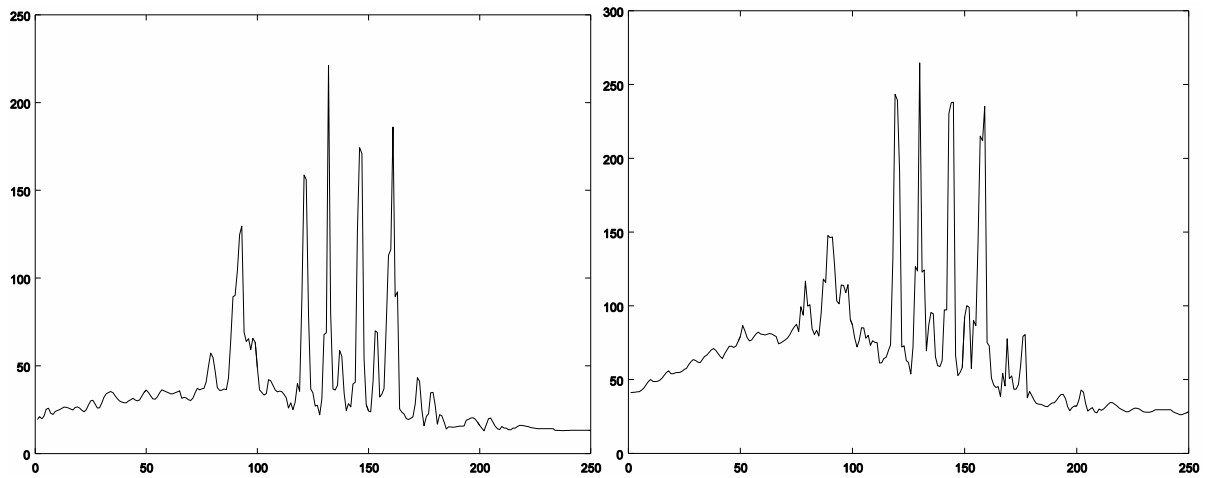
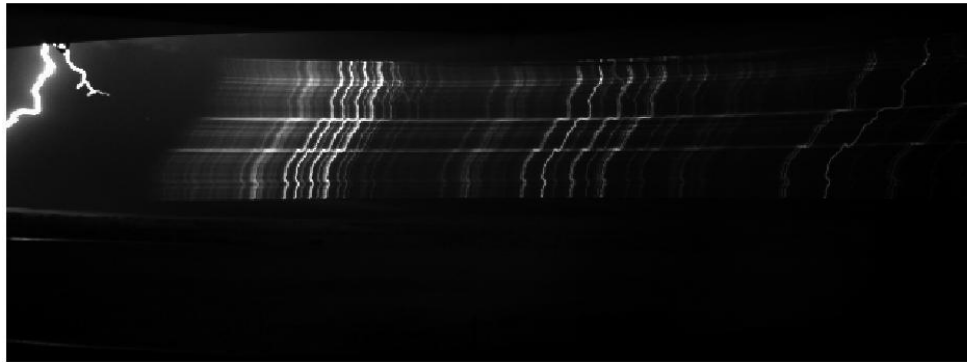


Fig. 5.1. The light spectra of a nature lightning flash recorded in USA.

5.2.2 Our plans for observations of lightning light spectra

Two high speed cameras will be used for light spectra observation with frame rate up to 500000 fps. One is used for measure the optical power and structure. The other combined with a grating records spectra evolution of lightning. A fast antenna and a slow antenna are applied to record the electrical and magnetic field.

Usually a lightning flash may include a number of return strokes, lasting less than 2 seconds. Each return stroke may last several hundreds of micro seconds. Therefore, to achieve the detail of a return stroke, a camera with capability of faster than 10k frames per second and record at least 2s is necessary.

Chapter 6. Conclusion and Discussion

Based on the macroscopic model concept of *Kumar et al. (2008)*, a modified electromagnetic-physical model for first lightning return stroke is proposed. The model is modified in following 4 aspects.

1) The bi-directional leader concept [*Chen et al., 2013*] and the attachment process [*Tran and Rakov, 2015*] are introduced into the model. The results of a self-organized downward negative leader (DNL) model [*Xu and Chen, 2013*] are applied as the initial state of the return stroke channel. For a given channel root potential in the cloud, the leader model provides parameters such as the striking distance and the current, longitudinal electric field, conductance, charge quantity and radius of the leader channel just before the return stroke, which are taken as the initial state of the return stroke channel. Besides, based on the difference of critical electric field between negative and positive polarities, an upward connecting leader (UCL) corresponding to a DNL is defined, and the two-current-wave phenomena (during the attachment process) at the return stroke starting stage is successfully simulated. It should be mentioned that the two-wave propagation phenomenon was well analyzed in works of *Raysaha et al. (2012)*, but for cases of lightning strokes to tall grounded objects. Our works here aims to make the modelling of leader, attachment and return stroke process be self-consistent.

2) The evolution mode of channel conductance, which is the most important parameter in the model, is further modified. *Kumar et al. (2008)* used the

Toepler's spark law and the first-order arc function for the channel conductance for the streamer and arcing regimes respectively. For rising current, they used equation $dg/dt = (g_{\infty}-g)/\vartheta_r$, but for falling current they used equation $dg/dt = -g/\vartheta_f$. This means that: (i) the channel conductance increases as the current increases and decreases as the current decreases, and (ii) the conductance is independent of the channel current at its falling stage, no matter it is below or above the g_{∞} at the moment. Since the both are empirical laws based on spark discharges in laboratory, modifications of them against lightning are necessary. Based on comparisons of simulated return stroke currents and those reported in the literature, we propose to use the same equation (26), $dg/dt = (g_{\infty}-g)/\vartheta$, for both the rising and falling stages of the channel conductance. This means that the conductance will keep to increase unless it becomes equal or larger than the g_{∞} at the moment. Besides, we propose to take the factor α in equation (27) as 1.0 and 0.2 for leader and return stroke channels respectively. Ranges of the simulated channel conductance with these modifications are qualitatively reasonable when compared with those in the literature.

- 3) The evolution of channel core radius versus the channel core conductance is introduced. The lightning channel core is consisted of high-temperature air plasma. The radius of the channel core depends on the plasma pressure, temperature and mass density of the core. In general, the return stroke channel core may have a nonlinear relationship that $PV \sim nRT$ (where, P - pressure, V - volume, T - temperature, and R – a constant related to specific gases, which might be a function of T when the temperature is very high) and P may tend to keep balance with the surrounding air. As the first-order approximation, we

assume that the R keeps constant and P and V are equally weighted versus T . The temperature links to the channel ionization degree and hence the conductivity, while the volume links to the channel core radius. As such, the channel core radius is related to the channel conductance as shown by equation (24). Such a linear gas approximation may lead to a slower expansion of the core radius than the reality. Further modification and testing of the equation (24) are needed.

- 4) An alternative digitizing and solving approach for the time domain electric field integral equation (TD-EFIE) is proposed. Since TD-EFIE includes both differential and integral terms and varies with both space and time, digitizing process of the equation has significant impact on the solution accuracy. A popular digitizing solution for TD-EFIE is the quadratic space and time interpolation function by *Miller et al. (1973)*, which can accurately evaluate the dependent variables in TD-EFIE at any point in the spacetime cone with a mild restriction on the space and time sample density. In the Miller's function, a singly connected wire structure is divided into a number of segments ($i = 1, \dots, N$), each with a space length of Δs and centered at s_i . The time domain is also divided into a number of elements ($j = 1, \dots, M$), each with a time interval of Δt and centered at t_j . A current I_{ij} is defined for the spacetime point centered at s_i and t_j . The current distribution within the segment i around time j , $I_{ij}(s', t')$ is then determined with the nine-point quadratic interpolation method in space and time dimensions. To avoid interpolation into the future, the current at time step j is interpolated backwards to time steps $j-1$ and $j-2$ when $(s' - s_i) / c\Delta t < 0.5$. Otherwise, the interpolation in time is from time step j to $j+1$ and $j-1$. The space interpolation is from segment i

to $i+1$ and $i-1$ [see page 31 of *Miller et al., 1973*]. As such, the self-term of current-time-derivative $(dl/dt)_{ij}$ for a segment at time j is actually expressed as a complicated function of the current in the concerned segment at times j , $j-1$ and $j-2$ as well as that in its neighbor segments. In contrast, in the present method, we use the conventional digitizing approach that the channel is directly divided into many small elements, each is assigned with a uniform current along the element. The time step Δt is strictly related to the space element Δs by $\Delta s = 2c\Delta t$ for better accuracy. In particular, both $(dl/dt)_{ij}$ and I_{ij} terms in the equation are kept as what they are to form a matrix differential equation like: $L_{ij}(dl/dt)_{ij} + Z_{ij}I_{ij} = E^A_i - E^C_{ij}$, as shown by equations (3.19 - 3.21). The I_{ij} can then be analytically solved out as a function of $(L_{ij}, Z_{ij}, E^A_i, E^C_{ij})$, as shown by equations (3.22 - 3.23). With such special treatments, the computing efficiency is significantly enhanced without losing the accuracy.

Besides, based on the current and conductance outputs of TD-EFIE model, an approach for simulating the electromagnetic field and optical signal of a return stroke is proposed and tested, as shown by equations (30~32) and equations (3.33 - 3.36), respectively. The simulated light waveform versus the current waveform can well explain the observation results of *Wang et al. (1999, 2005 and 2014)*.

Moreover, with above models, simulations of the current and electromagnetic and optical signals of a return stroke are performed for different initiation potentials in the range of -10 MV ~ -140 MV, resulting in different channel heights (ranging from 300 m ~ 20 km), current peaks (ranging from 2.6 ~ 209 kA), return stroke speed peaks (ranging from 0.2c ~ 0.8c) and light power peaks (ranging from 4.76 ~ 248

MW/m). The larger of the initiation potential, the larger of the channel height, current, return stroke speed and light power. Both the current peak and its propagation speed attenuate exponentially as it propagates upward. All these results are qualitatively and quantitatively consistent with those reported in literature [Guo and Krider, 1983; Quick and Krider, 2013; Shao et al., 2012; Wang et al., 1999 & 2005].

For future works,

- 1) The present model needs to be further completed to adapt different cloud potential and height of initial point. Since natural lightning has 3-dimensional structure and sometimes strike on the high buildings, these lightning flash under different conditions can be simulated based on the accomplished simple model.
- 2) Lightning light emission is formed by complex plasma molecular and atomic energy level transition process. If fusion plasma luminescence principle, luminescent model will be more accurate, consistent with the observed waveform.
- 3) Observations of the light spectra from lightning return strokes are necessary for validation of the model, particularly for the assumed channel conductance evolution mode. From the light spectra, one can get the channel temperature evolution, hence channel conductivity change.

Reference

- Baum, C.E., and L. Baker (1990), Analytic return-stroke transmission-line model, *In Lightning Electromagnetics*, ed. R.L. Gardner, pp.17-40, New York: Hemisphere.
- Berger, K. (1967) Novel observations on lightning discharges: Results of research on Mount San Salvatore. *Journal of the Franklin Institute* **283**, 478-525.
- Berger, K. (1975) Parameters of lightning flashes. *Electra* **41**, 23-37.
- Chen, M., and Y. Du (2009), Possible impacts of earthing path impedance on lightning return stroke currents, *HKIE Transactions*, **16(1)**, 7-13, doi.org/10.1080/1023697X.2009.10668145.
- Chen, M., X. Gou, and Y. Du (2013), The effect of ground altitude on lightning striking distance based on a bi-directional leader model, *Atmos. Res.*, **125-126**, 76-83.
- Chen, F. F., and A. Trivelpiece (1976), Introduction to plasma physics, *Physics Today*, **29**, 54.
- Cooray, V. (2014), The lightning flash, *The Institution of Engineering and Technology, London*.
- Devoto, R. S. (1967), Transport coefficients of partially ionized Argon, *The Physics of Fluids*, **10**, 354-364, doi: 10.1063/1.1762115.
- Du, Y., and M. Chen (2010), Influence of building structures on the lightning return stroke current, *IEEE Trans. on Power Delivery*, **25(1)**, 307-315, doi:10.1109/TPWRD.2009.2035420.

- Du, Y., X.H. Wang, and M. Chen (2012), Circuit parameter of vertical wires above a lossy ground in PEEC models, *IEEE Trans. on EMC*, **54**(4), 871-879, doi:10.1109/TEMC.2011.2174240.
- Dwyer, J. R., Uman, M. A., Rassoul, H. K., Al-Dayeh, M., Caraway, L., Jerauld, J., Rakov, V. A., Jordan, D. M., Rambo, K. J. & Corbin, V. (2003) Energetic radiation produced during rocket-triggered lightning. *Science* **299**, 694-697.
- Fuchs, F., Landers, E. U., Schmid, R. & Wiesinger, J. (1998) Lightning current and magnetic field parameters caused by lightning strikes to tall structures relating to interference of electronic systems. *Electromagnetic Compatibility, IEEE Transactions on* **40**, 444-451.
- Gorin, B. N., and V. I. Markin (1975), Lightning return stroke as a transient process in a distributed system, *Trudy ENIN*, **43**, 114-30.
- Guo, C. and E. P. Krider (1982), The optical and radiation field signatures produced by lightning return strokes, *J. Geophys. Res.: Oceans (1978–2012)*, **87**, 8913-8922.
- Guo, C., and E. P. Krider (1983), The optical power radiated by lightning return strokes, *J. Geophys. Res.: Oceans*, **88**, 8621-8622.
- Hutzler, B., and D. Hutzler-Barre (1978), Leader propagation model for predetermination of switching surge flashover voltage of large air gaps, *IEEE Trans. Power Apparatus and Systems*, 1087-1096.
- Idone, V. P. and R. E. Orville (1982), Lightning return stroke velocities in the Thunderstorm Research International Program (TRIP), *J. Geophys. Res.: Oceans (1978–2012)* **87**, 4903-4916.

- Kumar, U., R. B. Raysaha, and K. Kumar (2008), Time Domain Modelling of First Return Stroke of Lightning, *Open Atmos. Sci. Journal*, **2**, 261-270.
- Kumar, U., and R. B. Raysaha (2013), Genesis of return stroke current evolution at the wavefront, *Atmos. Res.*, **29**, 42-48.
- Inan, U. S., and M. Gołkowski (2011), *Principles of plasma physics for engineers and scientists*, xiv, 270 p. pp., Cambridge University Press, Cambridge ; New
- Lin, Y., Uman, M. & Standler, R. (1980) Lightning return stroke models. *Journal of Geophysical Research: Oceans (1978–2012)* **85**, 1571-1583.
- Ma, S., J. Howard, and N. Thapar (2011), Relations between light emission and electron density and temperature fluctuations in a helium plasma, *Physics of Plasmas*, **18**, 083301 (2011), doi:10.1063/1.3620403.
- Maslowski, G., and V. A. Rakov (2006), A study of the lightning channel corona sheath, *J. Geophys. Res.*, **111**, D14110, doi:10.1029/2005JD006858.
- Mazur, V., L. H. Ruhnke (1998), Model of electric charges in thunderstorms and associated lightning, *J. Geophys. Res.*, **103**, 23,299–23,308.
- McCann, G. (1944) The measurement of lightning currents in direct strokes, *Electrical Engineering*, **63**, 1157-1164.
- Miller, E.K., A.J. Poggio, and G.J. Burke (1973), An integral equation technique for the time-domain analysis of thin wire structure. Part I: The numerical method. *J. Comput. Phys.*, **12**, 24-48.
- Moini, R., V. A. Rakov, M. A. Uman, and B. Kordi (1997), An antenna theory model for the lightning return stroke, *Proc. 12th Int. Symp. On Electromagnetic Compatibility*, Zurich, Switzerland.

- Morris, J. C., R. P. Rudis, and J. M. Yos (1970), Measurements of electrical and thermal conductivity of Hydrogen, Nitrogen, and Argon at high temperatures, *The Physics of Fluids*, **13**, 608-617, doi: 10.1063/1.1692966.
- Olsen, H. (1959), Thermal and electrical properties of an argon plasma, *Physics of Fluids (1958-1988)*, **2**(6), 614-623.
- Orville, R. E. (1968), A high-speed time-resolved spectroscopic study of the lightning return stroke: Part I. A qualitative analysis, *Journal of the Atmospheric Sciences*, **25**(5), 827-838.
- Orville, R. E., and R. W. Henderson (1986), Global distribution of midnight lightning: September 1977 to August 1978, *Monthly Weather Review*, **114**(12), 2640-2653.
- Paul, C. R. (2008) *Analysis of multiconductor transmission lines*. John Wiley & Sons.
- Pinto, O., Pinto, I., Saba, M., Solorzano, N. & Guedes, D. (2005) Return stroke peak current observations of negative natural and triggered lightning in Brazil. *Atmospheric Research* **76**, 493-502.
- Plooster, M. N. (1970) Shock waves from line sources. Numerical solutions and experimental measurements. *Physics of Fluids (1958-1988)* **13**, 2665-2675.
- Plooster, M. N. (1971) Numerical simulation of spark discharges in air. *Physics of Fluids (1958-1988)* **14**, 2111-2123.
- Plooster, M. N. & Garvin, D. (1956) The Hydrogen-Bromine Reaction at Elevated Temperatures¹. *Journal of the American Chemical Society* **78**, 6003-6008.
- Podgorski, A. S. & Landt, J. A. (1987) Three-dimensional time domain modeling of

- lightning. *Power Engineering Review, IEEE*, 72-73.
- Popov, N. A. (2003), Formation and development of a leader channel in air, *Plasma Physics reports*, **29**, 695-708.
- Prueitt, M. L. (1963), The excitation temperature of lightning, *Journal of Geophysical Research*, **68**(3), 803-811.
- Quick, M. G., and E. P. Krider (2013), Optical power and energy radiated by natural lightning, *J. Geophys. Res.: Atmosphere*, **118**, 1868-1879.
- Raizer, Y. P. (1991), Gas Discharge Physics, *Springer-Verlag, Berlin*.
- Rakov, V. A. (1997), Lightning electromagnetic fields: modeling and measurements, *Proc. 12th Int. Symp. On Electromagnetic Compatibility*, Zurich, Switzerland, pp.59-64.
- Rakov, V. A. (1998), Some inferences on the propagation mechanisms of dart leaders and return strokes, *J. Geophys. Res.: Atmos.*, **103** (D2), 1879-1887, doi:10.1029/97JD03116.
- Rakov, V. A. and M. A. Uman (1998), Review and evaluation of lightning return stroke models including some aspects of their application, *IEEE Trans. EMC*, **40**, 403-426.
- Rakov, V. A., and M. A. Uman (2003), *Lightning: physics and effects*, pp.143-163, Cambridge University Press.
- Rakov, V. A. & Uman, M. A. (2007) *Lightning: physics and effects*. Cambridge University Press.

- Raysaha, R. B., U. Kumar, and R. Thottappillil (2011), A macroscopic model for first return stroke of lightning, *IEEE Trans. EMC*, **53**, 782-791. doi:10.1109/Temc.2010.2090663.
- Raysaha, R. B., U. Kumar, and V. Cooray (2012), Analysis for the reflected waves transmitted on to the channel by tall grounded objects using a special case, *IEEE Trans. EMC*, **54** (No.2), 262-271.
- Riaby, V. A., V. P. Savinov, A. V. Patziora¹, and D. P. Tkachenko (2010), Evaluation of the mean argon plasma conductivity and temperature at the exit of an atmospheric DC arc plasma torch, *Journal of Physics: Conference Series* **223**, 012007 (2010), doi:10.1088/1742-6596/223/1/012007.
- Riousset, J. A., V. P. Pasko, P. R. Krehbiel, R. J. Thomas, and W. Rison (2007), Three dimensional fractal modeling of intracloud lightning discharge in a New Mexico thunderstorm and comparison with lightningmapping observations, *J. Geophys. Res.*, **112**, D15203, doi:10.1029/2006JD007621.
- Rizk, F. A. M. (1989), A model for switching impulse leader inception and breakdown of long air-gaps, *IEEE Trans. Pow. Del.*, **4**, 596-606.
- Sadiku, M. N. (2007) *Elements of electromagnetics*. Oxford university press.
- Salanave, L., Orville, R. & Richards, C. (1962) Slitless spectra of lightning in the region from 3850 to 6900 angstroms. *Journal of Geophysical Research* **67**, 1877-1884.
- Shao, X.-M., E. Lay, and A. R. Jacobson (2012), On the behavior of return stroke current and the remotely detected electric field change waveform, *J. Geophys. Res.: Atmos.*, **117**, D07105, doi:10.1029/2011JD017210.

- Tran, M. D., and V. A. Rakov (2015), When does the lightning attachment process actually begin ?, *J. Geophys. Res.: Atmos.*, **120**, 6922-6936, doi:10.1002/2015JD023155.
- Uman, M. A. (2001) *The lightning discharge*. Courier Corporation.
- Wallace, L. (1964), The Spectrum of Lightning, *The Astrophysical Journal*, **139**, 994.
- Wang, D., N. Takagi, T. Watanabe, V. Rakov, and M. Uman (1999), Observed leader and return-stroke propagation characteristics in the bottom 400 m of a rocket-triggered lightning channel, *J. Geophys. Res.: Atmospheres*, **104**, 14369-14376.
- Wang, D., N. Takagi, T. Watanabe, V. A. Rakov, M. A. Uman, K. J. Rambob, and M. V. Stapleton (2005), A comparison of channel-base currents and optical signals for rocket-triggered lightning strokes, *Atmos. Res.*, **76**, 412-422.
- Wang, D., W. R. Gamerota, M. A. Uman, N. Takagi, J. D. Hill, J. Pilkey, T. Ngin, D. M. Jordan, S. Mallick, and V. A. Rakov (2014), Lightning attachment processes of an anomalous triggered lightning discharge, *J. Geophys. Res.: Atmospheres*, **119**(3), 1524-1533, doi:10.1002/2013JD020787.
- Xu, Y., and M. Chen (2013), A 3-D Self-Organized Leader Propagation Model and Its Engineering Approximation for Lightning Protection Analysis, *IEEE Trans. Pow. Del.*, **28**, 2342-2355. Doi:10.1109/tpwrd.2013.2263846.
- Zhou, M., D. Wang, J. Wang, N. Takagi, W. Gamerota, M. Uman, D. Jordan, J. Pilkey, and T. Ngin (2014), Correlation between the channel-bottom light intensity and channel-base current of a rocket-triggered lightning flash, *J. Geophys. Res.: Atmospheres*, **119**, 13457-13473.